Volume 93, Number 6, November-December 1988
Journal of Research of the National Institute of Standards and Technology

In This Issue:

EDITORIAL 635
Comments from the Chief Editor

Departments

News Briefs

DEVELOPMENTS 637
Exporters Urged to Follow Proposed EC Standards
Using Elevators for the Handicapped During a Fire
New Diagram for Predicting Weld Phases
High Accuracy Satellite Time Transfer
GOSIP Approved as Federal Standard
Expanded Coaxial Noise Calibration Available
U.S., Canada Laboratory Accreditation to Facilitate International Trade
Five NIST Projects Win 1988 R&D 100 Awards
U.S.-Japan Test Standards
Silicon Photodetector Self-Calibration Accuracy Verified in International Comparison
Wiggler for the NIST Free-Electron Laser

STANDARD REFERENCE MATERIAL 641
Standard Reference Material (SRM) 1879—Respirable Cristobalite

Articles

Kinetic Studies Using a Highly Sensitive Microphone Detector — **Walter Braun, Philippe Dagaut, and Barry C. Cadoff** 643

Solvent-Free Injection in Supercritical Fluid Chromatography Using Sintered Glass Deposition — **Thomas J. Bruno** 655

Paper from the Accuracy in Trace Analysis Symposium Proceedings not included in J. Res. Natl. Bur. Stand., Vol. 93, No. 3 (1988)

Enzyme-Enhanced Electrochemical Immunoassay for Phenytoin — **Mirtha Umaña, Jess Waller, Mansukh Wani, Carol Whisnant, and Edgar Cook** 659

Paper from the Accuracy in Trace Analysis Symposium Proceedings not included in J. Res. Natl. Bur. Stand., Vol. 93, No. 3 (1988)

Liposome-Based Flow Injection Immunoassay System — **Laurie Locascio-Brown, Anne L. Plant, and Richard A. Durst** 663

Conferences/Events

Workshop on Microstructure and Macromolecular Research with Cold Neutrons
National Bureau of Standards, Gaithersburg, MD, April 21–22, 1988 — **C. J. Glinka, J. A. Gotaas, and C. O'Connor** 667

U.S.-Japan Panel on Wind and Seismic Effects
National Bureau of Standards, Gaithersburg, MD, May 17–20, 1988 — **Noel J. Raufaste** 671

SUBJECT AND AUTHOR INDEX TO VOLUME 93 673

The National Bureau of Standards Becomes The National Institute of Standards and Technology

On August 23, 1988 President Reagan signed the Omnibus Trade and Competitiveness Act and changed the name of the National Bureau of Standards to the National Institute of Standards and Technology (NIST). Under a section of this new law known as the "Technology Competitiveness Act," several new assignments designed to boost U.S. industry in the world marketplace are added to the traditional functions of NIST.

NIST will continue to serve as the Nation's central laboratory for developing and disseminating measurement standards and scientific data for science, engineering, manufacturing, commerce, industry, and education. NIST will continue to provide a variety of services to the scientific and technical communities, including calibration services, standard reference data, and standard reference materials. These activities and the continuing research programs will continue to form the technical core of NIST.

New activities NIST has been assigned to develop are:

1. Create a series of Regional Centers for the Transfer of Manufacturing Technology that will be affiliated with non-profit institutions and organizations;
2. Develop a program to provide assistance and make Federal technology available to State and local technology programs and technology extension services;
3. Establish an Advanced Technology Program to encourage the commercialization of new high-technology products; and
4. Support a Department of Commerce Clearinghouse for State and Local Initiatives on Productivity, Technology, and Innovation to provide technical and analytical help to State and local officials making decisions on technology policy.

In keeping with the new name of our laboratories, we have changed the name of this journal to:

Journal of Research of the National Institute of Standards and Technology

Under its new name, this journal will continue its policy of presenting technical articles and news items of particular interest to scientists, technicians, and engineers interested in measurement methodology and analyses.

Karl G. Kessler
Chief Editor

Volume 93, Number 6, November–December 1988
Journal of Research of the National Institute of Standards and Technology

News Briefs

Developments

EXPORTERS URGED TO FOLLOW PROPOSED EC STANDARDS

The Commission of the European Communities (EC) is acting swiftly to turn the 12 member countries into a single integrated market of 320 million people by the end of 1992. EC legislation dealing with standardization is likely to have a profound effect on U.S. exports, predicts an NIST report. The report recommends U.S. business interests should establish communications with European subsidiaries, distributors, or their American industry associations to obtain up-to-date information on the development of European directives and standards. U.S. companies also are urged to seek and take opportunities to comment on, and attempt to influence, proposed European directives and standards. The NIST report contains a list of EC and U.S. government contacts for information on various aspects of EC activities related to standardization.

To obtain a copy of A Summary of the New European Community Approach to Standards Development (NBSIR 88-3793-1), send a self-addressed mailing label to: Patrick W. Cooke, Office of Standards Code and Information, A629 Administration Building, National Institute of Standards and Technology, Gaithersburg, MD 20899.

USING ELEVATORS FOR THE HANDICAPPED DURING A FIRE

Evacuating the handicapped during a fire has long been a concern to the fire protection community. Elevators would be an ideal solution, except for a number of fire-related problems including the "piston effect," which potentially can pull smoke and toxic gases into an elevator lobby as the elevator car moves upward. In a joint project, researchers at NIST and the National Research Council of Canada (NRCC) are developing smoke control technology for elevators and, most recently, analyzed the problem of piston effect. Several concepts for smoke control currently are being tested at NRCC's full-scale research tower. As part of the project, NIST and NRCC jointly will develop practical engineering design information for elevator smoke control.

NEW DIAGRAM FOR PREDICTING WELD PHASES

NIST researchers have produced a new, more accurate diagram for predicting the ferrite content of stainless steel welds. Knowledge of the ferrite content is important because, when held to within a certain small range, it helps to control the properties of the weld. Too low a ferrite content can cause cracking and too high a content can increase the rate of corrosion. The new diagram, developed in cooperation with the Colorado School of Mines and the Welding Research Council, was produced from a database containing more than 950 alloy composites from worldwide sources. It is more accurate than the two most commonly used diagrams, termed DeLong and Schaeffer.

For more information, contact Thomas A. Siewert, Fracture and Deformation Division, National Institute of Standards and Technology, Boulder, CO 80303.

HIGH ACCURACY SATELLITE TIME TRANSFER

Satellites have been used for over 25 years for dissemination of highly accurate time information. The coverage, however, has been restricted to certain areas of the Earth's surface. Now, NIST scientists can utilize several commercial communication satellites to disseminate a time signal whose eventual coverage will be worldwide. It will be an

extremely accurate signal—to within 1 nanosecond (1 billionth of a second). The experimental service was initiated recently using domestic U.S. satellites and will be extended to an Intelsat satellite; users require both a receiver and a transmitter. For more information, contact Dave Howe, Time and Frequency Division, National Institute of Standards and Technology, Boulder, CO 80303.

GOSIP APPROVED AS FEDERAL STANDARD

The Government Open Systems Interconnection Profile known as GOSIP was approved recently by the Secretary of Commerce as a Federal Information Processing Standard. (FIPS are developed by NIST for use by the federal government.) GOSIP defines a common set of data communication protocols which enable computer systems developed by different vendors to communicate and enable the users of different applications on these systems to exchange information. GOSIP is based on agreements reached by vendors and users of computer networks in workshops organized by the NIST National Computer and Telecommunications Laboratory.

Order FIPS PUB 146, Government Open Systems Interconnection Profile (GOSIP) from the National Technical Information Service, Springfield, VA 22161.

EXPANDED COAXIAL NOISE CALIBRATION AVAILABLE

NIST now can calibrate noise sources in the 8 to 12 GHz range for government and industry. The calibration is achieved using an automated radiometer and a cryogenic coaxial noise standard. With the addition, the system now routinely calibrates noise sources from 2 to 12 GHz at all frequencies and at all noise power spectral densities below 18,000 K. Measurement uncertainties range typically from 1 to 3 percent. In principle, there is no limitation on the type of coaxial connector. Current connectors are precision N, APC7, and GR900 as well as various rectangular waveguide flange connectors. The service is valuable to users since noise is the ultimate limiting factor in electromagnetic system performance. Manufacturers and users of high-precision electronic and communications equipment desire low-noise products so the products themselves don't distort the signal being generated, amplified, and received.

For more information contact George J. Counas, Division 723.02, National Institute of Standards and Technology, Boulder, CO 80303, 303/497-3664.

U.S., CANADA LABORATORY ACCREDITATION TO FACILITATE INTERNATIONAL TRADE

The U.S. National Institute of Standards and Technology (NIST) and the Standards Council of Canada (SCC) signed an agreement that will help reduce trade barriers between the world's two largest trading partners.

The agreement—signed by Ernest Ambler, NIST director, and John R. Woods, SCC executive director—provides mutual recognition of testing laboratories which are accredited by the NIST National Voluntary Laboratory Accreditation Program (NVLAP) and SCC National Accreditation Program for Testing Organizations (NAPTO).

The agreement is in accord with provisions of the assigned U.S.-Canada free trade agreement that is to go into effect January 1, 1989 pending approval by legislators in both countries. Under the free trade agreement, each party shall provide recognition of the accreditation systems for testing facilities, inspection agencies, and certification bodies of the other party.

The laboratory accreditation systems administered by NIST and SCC are voluntary; participation is not mandated by law in either country. NIST and SCC base their decision to accredit a testing laboratory on similar but not identical criteria. Officials responsible for administering each system have participated in assessment visits to testing laboratories accredited under the other national program.

The NVLAP program, established in 1976 and managed by the NIST Office of the Associate Director for Industry and Standards, is a voluntary "umbrella" system designed to assess the competence of laboratories to perform specific tests. "Competence" is determined by evaluating applicant laboratories to assure that they have the equipment, staff, and procedures necessary to perform prescribed tests in accordance with nationally or internationally accepted standards or test methods.

Currently, approximately 200 laboratories are accredited in programs administered by NIST for thermal insulation, carpet, solid-fuel room heaters, acoustical testing services, personnel radiation dosimeters, commercial products (paint, papers, and plastics), building seals and sealants, construction materials testing services, electromagnetic compatibility and telecommunications equipment, computer network protocols, and asbestos.

The Canadian NAPTO program was established in 1980. Formal recognition of competence in managing and performing specific tests has been granted to 49 private sector and government

laboratories in scientific, engineering and technological fields including: biological, chemical, electrical, mechanical, nondestructive, and physical and calibration testing. Testing organizations accredited under the SCC program form part of the National Standards System of Canada.

The agreement with the Standards Council of Canada is the fourth pact between NIST and a foreign laboratory accreditation system. NIST also has agreements with Australia's National Association of Testing Authorities, the National Testing Laboratory Scheme of the United Kingdom's National Physical Laboratory, and Testing Laboratory Registration Council of New Zealand.

For further information on NAPTO, or the NIST NVLAP program, contact: Manager, Laboratory Accreditation, A527 Administration Building, National Institute of Standards and Technology, Gaithersburg, MD 20899, 301/975-4016.

FIVE NIST PROJECTS WIN 1988 R&D 100 AWARDS

Five research projects in instrumentation and measurement technology from the Commerce Department's National Institute of Standards and Technology (NIST) received R&D 100 Awards.

R&D 100 Awards are bestowed annually by *Research & Development* magazine to highlight 100 significant technical products of the preceding year. NIST has now received 62 R&D 100 Awards since first entering the competition in 1973.

The 1988 award-winning projects include:

Optical Waveguide Dosimeter

William L. McLaughlin of the NIST Center for Radiation Research and Branislav Radak, a guest scientist from the Boris Kidric Institute in Yugoslavia, developed an extraordinarily versatile ionizing radiation dosimeter around the concept of radiation-sensitive dyes.

Colorless compounds that take on color when irradiated, "radiochromic dyes" have been in use for some years as one-shot, disposable dosimeters for industrial radiation processing, an application that McLaughlin pioneered.

In the new invention, the dyes are used in the core of a long fiber-optic tube that can be coiled into a small space, about 2 centimeters square. A light source at one end and a detector at the other read changes in the dye.

Because the light path can be quite long even in a small detector, the instrument can be made extremely sensitive. The optical waveguide dosimeters can function over a range from about 0.005 to 10,000 gray.

They will register either pulsed or steady radiation fields, and can measure accurately both dose and dose rates of x and gamma rays, neutrons, and charged-particle beams.

By selecting from a variety of available radiochromic dyes and plastics, researchers can tailor the dosimeters to have special properties, such as matching the radiation interaction characteristics of tissue for medical applications and radiation protection.

Cone Calorimeter

Vytenis Babrauskas and William Twilley of the NIST Center for Fire Research developed an apparatus which provides the data critical to predicting the fire hazard of a product from a small sample of material.

The instrument, known as the NIST Cone Calorimeter, measures the heat released and the rate at which it is released, the time it takes for a material to ignite, the amount of smoke produced, and the amount of several known toxic gases. Equipment previously available could not measure as many fire properties.

Both the ASTM and the International Organization for Standardization are proposing voluntary fire hazard test methods based on the NIST Cone Calorimeter. Commercial units now are sold by two U.S. manufacturers and a rapidly growing number are in use worldwide.

System for Absolute Determination of Aqueous Electrolyte Conductivity

Three NIST researchers constructed a device that determines the "absolute" electrical conductivity of aqueous (water-based) solutions and can be used as a primary standard against which other instruments may be compared.

The unique feature of the device is its measurement cell. Other available systems rely on cells of fixed geometry and work by comparing a solution of unknown conductivity to a standard calibration solution of known conductivity. These instruments typically are accurate to 0.1 percent.

The NIST system uses a variable cell size and does not have to be calibrated. Because its results are traceable to the physical standards of mass, length, and electrical resistance, the new device provides an "absolute" conductivity determination with an accuracy of 0.02 percent.

It also features extremely accurate temperature control, which is important because conductivity measurements are dependent on temperature.

The device has many potential applications. Standards laboratories desiring an absolute measuring system could adapt it. Other laboratories could use the device to calibrate existing conductivity measuring instruments. Oceanographers could employ it in measuring seawater salinity, and environmental scientists could determine dissolved solids.

With minor modifications, the device also could be used as a reliable indicator of water purity. Because contaminants change the electrical conductance of water, a measurement of a sample's conductance is a test of its purity. Such an instrument would be valuable in the pharmaceutical, electrical power, and electronics industries, which rely on pure water for their products.

The NIST system for absolute determination of aqueous electrolyte conductivity was developed by Drs. Yung Chi Wu, Kenneth W. Pratt, and William F. Koch, all of the NIST Center for Analytical Chemistry.

Trace Measurement System

Computers known as multiprocessors use more than one computing element, or "processor," to simultaneously solve many pieces of a problem. While multiprocessors can speed the processing of data, they also have unique problems including unbalanced processing loads, uneven flow of information, and an increased likelihood of communications bottlenecks.

Three researchers in the NIST National Computer and Telecommunications Laboratory developed tools to help measure the performance of multiprocessors. The ability to measure performance helps users evaluate and compare machines and manufacturers improve future designs.

Through a single circuit board added to the computer system, the Trace Measurement System (TRAMS), can measure key characteristics of a program such as the time it takes to execute a piece of code and how frequently a piece of code is executed.

Unlike other measurement systems now on the market, TRAMS is significantly simpler and, more importantly, does not disturb the operation being measured. Disturbances, or "perturbations," can alter the performance of a multiprocessor, making the results of the measurement meaningless.

NIST researchers Robert J. Carpenter, John W. Roberts, and Alan Mink developed the measurement system with partial sponsorship from the Defense Advanced Research Projects Agency.

Image-Preserving Optical Delay

Edward F. Kelley of the NIST Center for Electronics and Electrical Engineering generated a pioneering photographic "time machine" which, when used with a high-speed camera, permits photographing events which occurred before the camera's shutter is opened.

The system, called an image-preserving optical delay, differs from conventional photography which records an event only when the shutter is open.

This new device, an arrangement of optical components including mirrors and a crystal shutter, allows researchers to take detailed, high-speed photographs of random—that is, non triggered—events.

It is now used for processes which last from 100 nanoseconds, or billionths of a second, to 10 microseconds, or millionths of a second, to study materials utilized by the electric power industry.

This system stores optical images of a random event long enough so the shutter of a high-speed camera can be opened and photographs taken of the processes leading to the random event. Kelley has filed a patent application on the system.

Functionally, the optical delay is equivalent to forcing the image to travel an additional 120 meters before it gets to the camera. Using a series of concave and planar mirrors, this path length is folded into about 4 meters.

The system is rugged enough to be used in a variety of settings. Situated on a table-top, the device contains optical components which require alignment. However, normal vibration, air currents, and airborne dust have minimal effect on the system's operation. Also, the system does not require a clean room, an optical bench, or any other special features.

U.S.-JAPAN TEST STANDARDS

NIST, in cooperation with Japanese organizations and the American Society for Testing and Materials (ASTM), is developing standard test methods for measuring the tensile and fracture toughness properties of steels at liquid helium temperature (4 K). Special considerations apply to mechanical tests near absolute zero because of severe adiabatic heating during plastic deformation. The U.S. Department of Energy and the Japanese Atomic Energy Research Institute are supporting this work to develop design standards for fusion energy applications. The tensile and fracture standards are now in their sixth drafts and have been submitted to ASTM for formal approval.

SILICON PHOTODETECTOR SELF-CALIBRATION ACCURACY VERIFIED IN INTERNATIONAL COMPARISON

Silicon self-calibration, an accurate and convenient approach to photodetector spectral responsivity calibration founded on the fundamentals of solid state physics, has been successfully implemented at NIST and six other national laboratories as their absolute radiometric base. This technique was developed in 1980 by the Radiometric Physics Division.

The first intercomparison of spectral responsivity scales (or equivalently, monochromatic radiant power scales) that has occurred since a number of national laboratories adopted the new technique has been published recently in the report of the 11th session of the CIPM Consultative Committee for Photometry and Radiometry (CCPR). The comparison, which was run by NIST for the CCPR, included 11 national laboratories. Six used the silicon self-calibration method, four used electrical substitution radiometers, and one used both approaches to realize their scales of absolute spectral responsivity. The results showed that eight of the laboratories agree to within ± 0.15 percent in measuring the responsivity of two different silicon photodiodes at the 633 nm HeNe laser wavelength. This level of agreement is a factor of four better than the ± 0.6 percent achieved by six of the eight national laboratories in an earlier (1967) comparison.

WIGGLER FOR THE NIST FREE-ELECTRON LASER

The Radiation Source and Instrumentation Division recently signed a contract for installation of a wiggler. The wiggler is under construction and scheduled to be installed at NIST in October 1989. It is one of the key parts of the free-electron laser (FEL) facility being constructed as a joint project with the Naval Research Laboratory. The wiggler is a precise array of magnets with alternating fields that cause an electron beam to follow a sine trajectory and to emit intense, coherent radiation. This wiggler will be 3.64 m long and will have 130 magnetic periods. The electron beam will be provided by the racetrack microtron (RTM), which is nearing completion.

The NIST FEL facility will be the most versatile in the country, providing a very large range of wavelengths (200 nm to 10 μm) over which it will be continuously tunable. The FEL output will consist of a continuous train of 3-ps wide pulses at 74.375 MHz with an average power of 10 to 100 W. The facility will be operated for research in physics, chemistry, biophysics, and biomedicine.

Standard Reference Material

STANDARD REFERENCE MATERIAL (SRM) 1879—RESPIRABLE CRISTOBALITE

The various crystalline phases of silicon dioxide cause different physiological effects in the respiratory system and it is necessary to identify the crystalline phases in the industrial atmosphere to assess and monitor health risks. Standards of pure crystalline phases are needed to determine their presence by x-ray diffraction techniques.

The Office of Standard Reference Materials announces the availability of a respirable cristobalite powder certified for use as a quantitative x-ray powder diffraction standard. The powder is 98 percent crystalline cristobalite with no other detectable crystalline phases. The mass median equivalent spherical diameter of the powder is 3.3 microns, with 80 percent of the mass of the particles in the range of 2 to 5 microns.

This SRM and SRM 1878, Respirable Alpha Quartz, provide two respirable powders of different crystalline phases of silicon oxide. The program for the certification of these SRMs was begun in cooperation with the National Institute of Occupational Safety and Health.

Certification of this SRM was performed in the Ceramics Division of the Institute for Materials Science and Engineering.

Volume 93, Number 6, November–December 1988
Journal of Research of the National Institute of Standards and Technology

Kinetic Studies Using a Highly Sensitive Microphone Detector

Volume 93 Number 6 November–December 1988

Walter Braun, Philippe Dagaut, and Barry C. Cadoff

National Institute of Standards and Technology
Gaithersburg, MD 20899

A very sensitive microphone detector is used to study fast kinetic rate processes in the gas phase resulting in the generation of heat. The rate of heat evolution in turn produces a short duration pressure pulse which drives the microphone. The frequency response of the microphone is somewhat slower than required to record these pulses as they actually appear at the detector. The theory of the method used for the data reduction is presented. It is based upon the Green's Function method which expresses the time dependent microphone signal, X, (t), as the convolution of the pressure pulse function, $f(t)$, by the microphone's impulse response function, $G(t)$. A Fourier analysis of $X(t)$ and the two relevant functions, $f(t)$ and $G(t)$, at a single frequency, allows direct determination of the rate constant for the kinetic process under study. The method is demonstrated by applying it to the study of vibrational energy relaxation of pentafluorobenzene in argon buffer gas and gives results in agreement with other experimental methods.

Key words: CO_2 laser; energy transfer; gas phase; kinetics; measurement; optoacoustic; waveform analysis.

Accepted: June 9, 1988

1. Introduction

Several direct methods have been used to study energy transfer (relaxation) processes from vibrationally excited molecules in the gas phase. These methods can be distinguished by the way the vibrationally excited molecules are produced and how they are detected. Production methods include i), electronic excitation via pulsed excimer lasers, followed by rapid internal conversion into vibrational energy or ii), direct vibrational excitation using a pulsed CO_2 laser. Detection methods involve real-time measurement of the relaxation process through the use of a number of different energy detection probes: ultraviolet absorption, infrared absorption, infrared fluorescence, pressure wave detection (optoacoustics or interferometry), and broadening of Hg 254 nm absorption. Most of these energy detection methods are well suited to detecting relaxation in pulsed CO_2 laser experiments when the fluence of the laser is greater than about 0.25 J/cm^2. In experiments using excimer laser excitation the fluence is usually considerably attenuated in order to minimize photolysis by multi-photon absorption processes, resulting in a poorer signal-to-noise ratio.

Of all the detection methods employed, optoacoustic techniques (using microphones or piezoelectric crystals) are probably the most sensitive. However, microphones used in such experiments generally have a limited frequency response thereby confining measurements to systems exhibiting relatively slow energy relaxation [1]. The low pressure limit for performing such experiments is usually about 1 torr. Below this pressure the onset of dispersion (energy loss) due to diffusion and thermal conductivity results in a decreased signal.

The limitation of being able to measure only slow relaxation processes has recently been circumvented by Beck, Ringwelski, and Gordon (BRG) [2]. These workers employ a small surface area piezoelectric crystal detector with a high-frequency response. Their method involves the direct monitoring of individual pressure pulses arriving at the detector as a result of the pulsed CO_2 laser excitation of a gas. The pressure pulse is characterized by both a condensation (compression) and a rarefaction portion and their relative magnitudes is determined by the rate of energy relaxation, the size of the irradiated zone, the radiation distribution within this zone, and the speed of sound in the gas medium. The important advantage of faster response time has, however, incurred the disadvantage of lower detection sensitivity.

In this paper we explore the application of a very sensitive microphone detector to the measurement of relaxation rates that are somewhat faster than the angular frequency response of the detector. The measurements basically involve the sampling of amplitude information as well as some limited waveform information [3]. As in the BRG [2] experiments, individual pressure pulses are monitored. These pulses are not viewed as they actually appear at the detector but rather as the detector responds to them. The detector generally develops a damped ringing sine wave at a single angular frequency, ω_0, termed the characteristic or natural frequency. If ω_0 is much lower than the frequency of the pressure pulse then the pulse shape cannot be effectively extracted; however, amplitude and some waveform information remain so that it is still possible to measure accurate rate constants for vibrational relaxation processes faster than ω_0.

Thus, the measurable range of rate constants with the present method is about the same as with the BRG [2] method. This range is limited by the approximate condition $c_0/(10r_0) \leqslant k'P \leqslant 3c_0/r_0$, where k' is the bimolecular rate constant for energy relaxation (torr s)$^{-1}$, P is the bath gas pressure (torr), c_0 is the speed of sound in the bath gas medium (cm/s), and r_0 (cm) is the radius of the cylindrical zone irradiated by the excitation laser beam. The upper limit for measurable $k'P$ values is approximately the reciprocal of the time it takes for a pressure pulse to traverse the diameter of the irradiated zone; the lower limit comes about because late contributions to the developing pressure wave (due to slow relaxation) ultimately interfere with earlier contributions and the resultant pressure pulse is strongly attenuated (de-phased).

2. Theory of the Method

2.1 Background

We initially follow the procedure of Rothberg et al. [4] who described the use of microphones to perform photoacoustic calorimetry. Kinetic rate constants were not obtained by these workers, but an analysis was made on how very rapid or very slow kinetic processes (compared to ω_0) affect the microphone's sensitivity. In addition, their work dealt with pulsed laser excitation of liquid phase systems while here we concentrate entirely on the gas phase.

For convenience, in the following discussion the symbol t is to be viewed as a retarded time. It is a measure of time that begins ($t=0$) when the pressure pulse, originating from the laser irradiation zone, arrives at the detector.

We first deal with a simple model of the detector which is taken to be that of a damped harmonic oscillator [5] and follows the differential equation,

$$u(\mathrm{d}^2X/\mathrm{d}t^2)+v(\mathrm{d}X/\mathrm{d}t)+wX=f(t)\,, \tag{1}$$

where X is the displacement of the mechanical diaphragm from its equilibrium position, u is the diaphragm mass, v is a damping constant, and w is a spring constant. The functional form of a driving pressure pulse acting on the detector face as a function of time t, will here and in the rest of the text be given by the designation, $f(t)$. We now employ the Green's function method [6] to obtain the detector's response to the driving pressure pulse. We take this to be equal to $X(t)$ which is given by

$$X(t)=\int_0^t G(t,\tau)f(\tau)\,\mathrm{d}\tau=G*f\,, \tag{2}$$

where

$$G(t,\tau)=A\,\sin(\omega_0(t-\tau))\exp(-\beta(t-\tau)) \tag{3}$$

is the suitable Green's function for the initial value problem given by the differential eq (1) (assuming that $X=0$ and $\mathrm{d}X/\mathrm{d}t=0$ at $t=0$) and represents the impulse response function. Equation (3) describes an underdamped sine wave where A is an arbitrary amplitude constant and β is the damping constant. The detector response, given by eq (2) is thus the convolution of the pressure wave pulse incident on the detector, given by $f(\tau)$, by the impulse response, $G(t,\tau)$ and the convolution is designated by $(G*f)$. It is understood from the limits of integration in eq (2) that $G(t,\tau)$ is given by eq (3) for $\tau \leqslant t$ but is zero for $\tau > t$. Thus, if both f and G are known, the signal given by the detector is

completely specified by eq (2). The problem, in fact, can be completely solved experimentally: if a known pressure signal $f(t)$ is presented to the detector and its response $X(t)$ is measured, the function G can be determined through a deconvolution process. This is in principle possible through fast Fourier transform methods (FFT). Taking the Fourier transform of eq (2) gives, by the "Convolution Theorem,"

$$F[X(t)]=F[G(t)]\cdot F[f(t)]\,, \tag{4}$$

that is, the Fourier transform of the convolution is the product of the individual Fourier transforms. It remains to divide $F[X(t)]$ by $F[f(t)]$ and then, taking the inverse transform to recover $G(t)$. Once $G(t)$ is known, we can, in principle, recover $f(t)$ for any unknown pressure signal. However, we should point out that the duration of pressure wave $f(t)$ (see below) is frequently less than half of the period of the detector's impulse response so that such a deconvolution would not be expected to cleanly recover the shape of $f(t)$. This fact, coupled with inherent noise in the data and the use of an imperfect representation for $G(t)$ can frequently produce unsatisfactory results. For this reason we reduce our data in a somewhat different way which we develop in the succeeding sections.

2.2 Development of Present Method

It would be helpful if we could separate the quantities f and G out from within the integral in eq (2). This can be achieved by taking either a single-frequency [7] Laplace or Fourier transform of eq (2). Subsequently, we will consider the latter transform as a special case of the former. Taking the Laplace transform of the convolution function as the product of the individual Laplace transforms of $G(t)$ and $f(t)$,

$$L[X(t)]=L[G(t)]\cdot L[f(t)]\,, \tag{5}$$

results in

$$\int_0^\infty X(t)\exp(-\alpha t)\mathrm{d}t = \int_0^\infty G(t)\exp(-\alpha t)\mathrm{d}t\cdot\int_0^\infty f(t)\exp(-\alpha t)\mathrm{d}t. \tag{6}$$

Here α is an arbitrary real and positive constant. Using the function G, given by eq (3), the integral containing G in eq (6) is given by

$$\int_0^\infty G(t)\exp(-\alpha t)\mathrm{d}t=\omega_0/[(\alpha+\beta)^2+\omega_0^2]\,. \tag{7}$$

We have thus achieved the desired separation of the two functions G and f in eq (2). For the special (but frequently encountered) case where the functional form of $G(t)$ remains unchanged over a range of experimental conditions, eq (6) becomes,

$$\int_0^\infty X(t)\exp(-\alpha t)\mathrm{d}t = \text{constant}\cdot\int_0^\infty f(t)\exp(-\alpha t)\mathrm{d}t\,. \tag{8}$$

It then remains to reduce the actual data according to the first integral in eq (8) and calculate the second integral from known representations of $f(t)$. These representations will, as mentioned above, be a function of the irradiation geometry and the relaxation rate constant.

The time-varying pressure, at an observation point somewhat distant from the cylindrical axis of a laser irradiated zone, as obtained from the solution of the linearized acoustic wave equation, has been given by Bailey et al. [8], with some generalization by BRG [2]. We present the results of these two papers here in a notation similar to that of BRG [2],

$$f(\bar{t})=Q_0\,\bar{k}\int_0^\infty(\bar{l}^2+\bar{k}^2)^{-1}\{-\bar{k}\exp[-\bar{k}(\bar{t}+\bar{\delta})] +\bar{l}\sin[\bar{l}(\bar{t}+\bar{\delta})]+\bar{k}\cos[\bar{l}(\bar{t}+\bar{\delta})]\} J_0(\bar{l}\,\bar{r}_\mathrm{p})\,h(\bar{l})\bar{l}\mathrm{d}\bar{l}\,. \tag{9}$$

At this point we will be dealing with dimensionless quantities; the advantage of doing so will become clearer as we proceed. Also, for the sake of clarity a bar will be placed over all dimensionless quantities. In eq (9), dimensionless time is defined as $\bar{t}=tc_0/r_0$; dimensionless probe position is defined as $\bar{r}_\mathrm{p}=r_\mathrm{p}/r_0$; dimensionless pseudo-first-order rate constant $\bar{k}$ is given by $\bar{k}=kr_0/c_0$. The dimensional quantities consist of r_0 and c_0, defined earlier; r_p, the probe position which is the distance of the microphone from the axis of laser beam, always $\geqslant r_0$; k, the pseudo-first-ordered rate constant for energy relaxation (s^{-1}). This form allows us to arrive at any set of solutions regardless of the irradiation geometry and sound speed. The delay between the laser pulse and the arrival of the pressure wave at the detector is given by, $\bar{\delta}=(r_\mathrm{p}-r_0)/r_0$. In eq (9), $h(\bar{l})=\bar{J}_1(\bar{l})/\bar{l}$ characterizes a uniformly irradiated "tophat" geometry [9], J_0 and J_1 the zero and first

order Bessel functions, respectively, and Q_0 is a constant. Two examples of calculated pressure waves obtained under rapid relaxation and slow relaxation conditions are shown in figure 1.

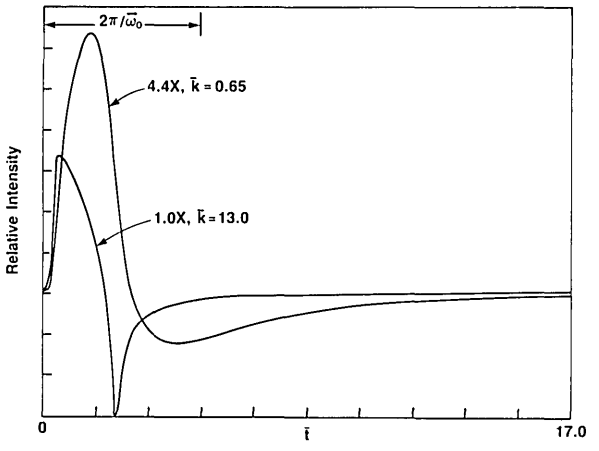

Figure 1. Two representative waveforms (in dimensionless units) of the pressure wave calculated from eq (9)—one for rapid relaxation, $\bar{k}=13$, and one for slower relaxation, $\bar{k}$-0.65. These two curves show approximately the full time span of the waveforms encountered under fast and relatively slow relaxation conditions. Curves are scaled by the factors indicated. The duration of one cycle of the microphone's damped impulse response function, $G(t)$ is shown for reference as $2\pi/\bar{\omega}_0$.

2.3 Calculation of Calibration Curves

It remains to determine the integral on the right-hand side of eq (8) as a function of a variable relaxation rate constant. This integral, expressed in terms of dimensionless time, $\bar{t}$; dimensionless rate constant, $\bar{k}$, and dimensionless alpha, defined as $\bar{\alpha}=\alpha r_0/c_0$, is given by,

$$L[f(\bar{t},\bar{k})]=\int_0^\infty f(\bar{t},\bar{k})\exp(-\bar{\alpha}\,\bar{t})\mathrm{d}\bar{t} \qquad (10)$$

Several curves were evaluated by numerically solving eq (10) using the expression for $f(\bar{t})$ given by eq (9), as a function of $\bar{k}$, for several values of $\bar{\alpha}$. There is some small error involved in the numerical integration. Within this minor limitation we fit these curves (normalized to unity for the fastest relaxation rate constant) to the following empirical expression,

$$L[f(\bar{t},\bar{k})] \propto 1-\exp(-\bar{a}\,\bar{k}^{0.75}). \qquad (11)$$

For reference, these curves are presented in figure 2. It should be noted that there may be no physical significance to the functional form given by eq (11), except that it best fits the results of the numerical integration of eq (10). Replacing the 0.75 exponent by unity results in a poorer fit. The significance of $\bar{\alpha}$ should be addressed at this point. It could first of all be viewed as a mathematical convenience allowing separation of the two terms, f and G, within the integral in eq (2). Alternatively the factor $\exp(-\alpha\bar{t})$ in eq (10) could be viewed as a "time window" used to crudely sample the shape of the pulse (waveform) in the chosen time domain. It is ultimately expected to distinguish between different waveforms with an accuracy sufficient to return meaningful kinetic results. As we discuss below it may or may not be adequate for the problem at hand.

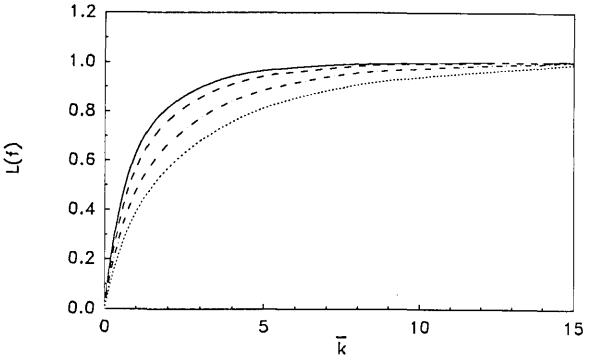

Figure 2. Several fits of $L[f(\bar{t})]$ eq (10) to the functional form of eq (11) for different values of α.

- - - , $\bar{\alpha}$=0.8122, $\bar{a}$=0.85
——— , $\bar{\alpha}$=0.4060, $\bar{a}$=1.00
-·-·- , $\bar{\alpha}$=0.0812, $\bar{a}$=0.65
· · · · · , $\bar{\alpha}$=0.0406, $\bar{a}$=0.50

The results of figure 2 show that, while α varies by about a factor of 20, the calibration factor, $\bar{a}$, varies by only a factor of two. In order to apply this methodology it is important to note that whatever the value of $\bar{\alpha}$ used to process the actual data, the same value for $\bar{\alpha}$ must be used to calculate the appropriate calibration curve.

2.4 Analysis of Experimental Waveforms

We ultimately perform experiments in which a pseudo-first-order relaxation rate constant is varied linearly through a change of the bath gas pressure. The experimental signal curve is processed according to the left-hand side of eq (8),

$$L[X(\bar{t},\bar{k})]=\int_0^\infty X(\bar{t},\bar{k})\exp(-\bar{\alpha}\,\bar{t})\mathrm{d}\bar{t}.$$

These results must also fit the functional form (normalized to unity) of eq (11),

$$L[X(\bar{t},\bar{k})] \propto 1-\exp(-AP^{0.75}) . \quad (12)$$

The experimental parameter, A, is thus derived from the experimental data. If the functional form of $G(\bar{t})$ remains constant, eqs (11) and (12) can simply be related according to eq (8) resulting in

$$1-\exp(-\bar{a}(\bar{k}'P)^{0.75})=1-\exp(-AP^{0.75}) , \quad (13)$$

where $\bar{k}'=\bar{k}/P$ is the dimensionless rate constant per unit pressure (bimolecular rate constant). If the functional form of $G(t)$ varies, eq (13) is still applicable, as discussed in section 4. However, the left-hand side of eq (12) must be replaced by $L(X)/L(G)$. That is, the variation of $L(G)$ must be taken into proper account. From eq (13), we arrive at

$$\bar{k}'=(A/\bar{a})^{1/0.75} . \quad (14)$$

Equation (14) thus involves the experimental parameter, A, and the appropriate calibration factor, $\bar{a}$. The dimensional rate constant per unit pressure, k', is related to the dimensionless rate constant per unit pressure, $\bar{k}'$, according to

$$k'=\bar{k}' \, (c_0/r_0) . \quad (15)$$

We have evaluated $f(\bar{t})$ assuming that the microphone is a point detector. It actually occupies a finite width, d_0, in the radial direction of the propagating pressure wave. Thus the function, $f(\bar{t})$, should be convolved using the suitable rectangular slit function (function of $\bar{d}_0=d_0/c_0$). However, we here make the ad hoc assumption that the convolving effect of d_0 on $f(t)$ is quite analogous to the effect on $f(t)$ produced by a simple increase in the diameter of the laser beam, $2r_0$, which should be a good approximation if $d_0 \leqslant 2r_0$. Equation (15) is then modified to its final form,

$$k'=\bar{k}' \, c_0(r_0+d_0/2)^{-1}=\bar{k}' \, c_0/r_{0\,(\mathrm{eff})} , \quad (16)$$

where an effective r_0 is calculated as indicated.

2.5 Fourier Transform Method

An entirely analogous treatment can be applied to the case of a Fourier transform viewed as a special case of a Laplace transform. Then for $\alpha=-i\omega$, where $i=\sqrt{-1}$, ω being an arbitrary positive frequency, we refer back to eq (4), where it is understood here that we are transforming only at a single frequency, that in evaluating $F(X)$, $F(G)$ or $F(f)$ the integration over time extends from zero to infinity, and that the transformed result is in the complex plane.

When $\alpha=i\omega$ eq (4) becomes

$$F^*(X)=F^*(G)F \cdot F^*(f) . \quad (17)$$

The product of eqs (4) and (17) returns a result which is a real number

$$F(X) \cdot F^*(X)=F(G) \cdot F^*(G) \cdot F(f) \cdot F^*(f) . \quad (18)$$

Equation (18) is entirely rigorous whether $G(t)$ remains constant or not. However, if $G(t)$ is constant then the Fourier transform of $X(t)$ multiplied by its complex conjugate is simply proportional to the Fourier transform of the function $f(t)$ multiplied by its complex conjugate.

We now develop a set of calibration curves by calculating $F(f) \cdot F^*(f)$ which are the Fourier analogues of the Laplace calibrations depicted in figure 2. These are presented in figure 3 for reference.

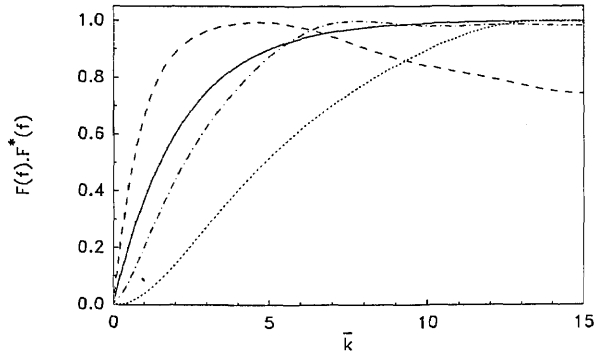

Figure 3. Numerical calculations $F(f) \cdot F^*(f)$, eq (18), for the conditions $\bar{\omega}=1.256$ and

- - - - , $0.5\bar{\omega}$
-·-·- , $2.0\bar{\omega}$
· · · · · , $4.0\bar{\omega}$
——— , $1.0\bar{\omega}$ as fit to eq (19) with $\bar{a}=0.46$.

While a number of curves for variable α can be fit to the functional form of eq (11) for the Laplace transform case, here for the case of the Fourier transform multiplied by its complex conjugate, only a range of $\bar{\omega}$ values can be accurately fit by the following simple functional form,

$$F(f) \cdot F^*(f)=1-\exp(-\bar{a}\,\bar{k}) . \quad (19)$$

In all other respects the treatment given above applies to the present case, with the one exception that wherever the exponent 0.75 appears in an equation it is to be replaced by unity. Also, eq (19) should be used only for values of $\bar{\omega}$ around 1.0; for other values of $\bar{\omega}$, the other curves shown in figure 3 should be cast in suitable functional forms and counterpart experimental results analyzed in the same way.

2.6 Method Summary

The procedure outlined above involves taking suitable transforms, i) of the pressure wave as a function of the pseudo-first-order relaxation rate constant, ii) of $G(t)$, if its functional form varies over the range of experimental conditions and finally, iii) of the experimental data as a function of the bath gas pressure. The processed results, when expressed in terms of the appropriate analytical functional form, allow simple extraction of the energy relaxation rate constant. Each operation involves taking a single-value transform. This accurately samples the amplitude and also samples the waveform in sufficient detail to produce accurate kinetic results.

The alternative procedure using FFT methods, as mentioned earlier, is subject to failure under the present conditions (at least with respect to recovering a precise waveform) and further requires the tedious task of making additional waveform comparisons in order to finally extract a relaxation rate constant.

3. Experimental Procedure

The essential features of the experiment are presented schematically in figure 4. A CO_2 TEA laser delivering about 0.5 J/cm^2 per pulse of about 200 ns duration is directed into the spherical absorption chamber through a variable iris as a quasi-parallel beam. The diameter of the laser beam is adjustable from about 2 to 10 mm. A Knowles microphone BT-1759 was used in the present work [10]. The approximate dimensions, orientation and position of the microphone are given in figure 4. The device consists of a rectangular thin-metal diaphragm placed in close proximity to an electret disk behind which is positioned a ceramic printed circuit (PC) board containing an internal amplifier. This assembly is potted within a thin metal casing, the face of which contains several rows of holes which allow the diaphragm to respond to pressure changes in the environment. An equivalent electrical circuit describing the microphone consists of a battery

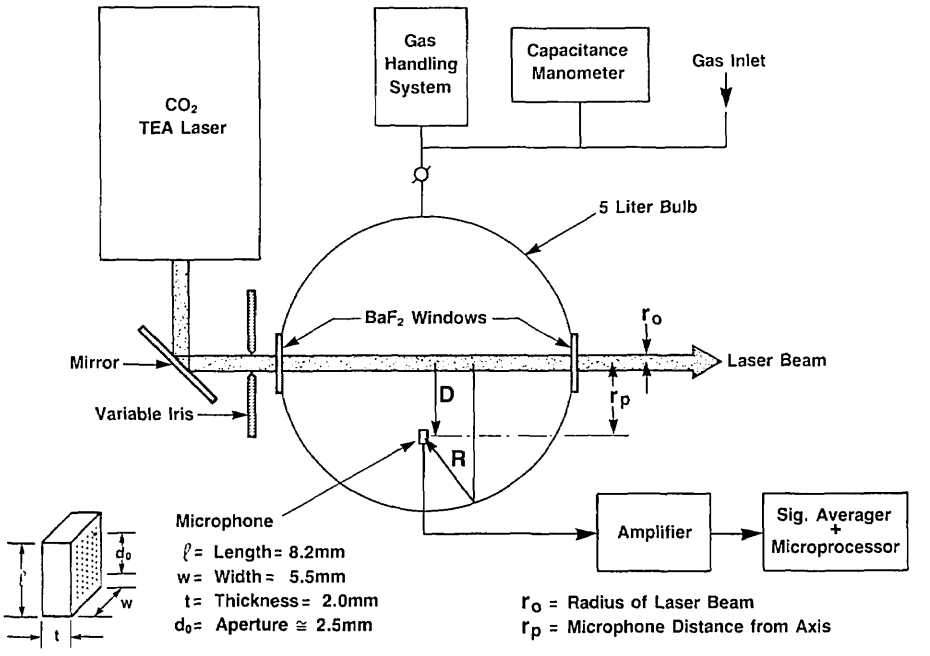

Figure 4. Schematic diagram of apparatus showing microphone position and approximate dimensions. The symbols D and R designate the direct (primary) and reflected pressure waves, respectively.

connected in series with a variable capacitance (the diaphragm) which is connected to the PC amplifier assembly. The assembly is biased with an external 1.35 V battery. The output of the microphone amplifier is connected with a short cable to an additional pre-amplifier which is used to reduce the output impedance of the microphone from about 3.5 kΩ to 50 Ω. The signal from this pre-amplifier is then fed to a Tektronix Model AM502 high-gain differential amplifier, the frequency response of which is set for a low-frequency 3-db cut-off of 10 KHz and a high-frequency 3-db cut-off of 1 MHz.

The output of this high gain amplifier is then connected to a Biomation Model 8100 fast digitizer which transmits the signal through an interface to the microcomputer assembly. The fast digitizer is triggered by a trigger pulse generated at the beginning of each CO_2 laser pulse. The microphone signal to the fast digitizer is further retarded by a pre-set time delay equal to or less than the time required for the pressure wave to travel from the laser-irradiated zone to the microphone detector. Multiple laser shots could thus be accumulated (averaged), viewed in real time, and finally stored on disks for further data reduction.

A typical set of experiments consists of i) preparing a dilute mixture (less than about one part per thousand) of an infrared absorbing gas in a non-absorbing diluent gas, in the 5-liter vessel containing the microphone assembly; ii) subjecting the mixture, at some total pressure, P, to one or more CO_2 laser pulses, simultaneously recording the microphone signal response and then storing the resultant waveform; iii) reducing the pressure of the mixture in stages, each followed by laser excitation and data aquisition, in order to follow the kinetics of the relaxation process. The resultant waveforms are finally processed according to the method presented in the previous section. Further details are given in section 4.

The gas handling system could be evacuated to pressures less than 1×10^{-6} torr. The infrared absorbing gas used in the present work was pentafluorobenzene (PFB) and the diluent gas was argon. Pressures were measured with a calibrated capacitance manometer. Gas mixtures were introduced at pressures down to about 0.5 torr and could be measured to better than 0.01 torr with the pressure measuring head.

4. Results

4.1 Microphone Response Function, $G(t)$

Before analyzing a typical energy relaxation experiment, we first describe several tests performed on the microphone assembly to determine its operating characteristics. These characteristics basically determine the functional form of $G(t)$. Whatever the functional form of $G(t)$, it is important that it either remain constant under the varying conditions of a set experiments, or if it varies, that its transform be independently obtained.

We first attempt to deduce an approximate functional form of $G(t)$ for the specific microphone detector employed in these experiments and we then determine if $G(t)$ varies under changing experimental conditions.

A computer algorithm was prepared to numerically perform the convolution given by eq (2). When we convolved $G(t)$, given by eq (3), with a variety of simple pressure pulses, $f(t)$, we obtained waveforms exhibiting the same characteristic feature: the first maximum was always significantly larger than the absolute value of the first minimum. The reverse effect was always observed for the experimental waveforms. Replacing eq (3) by

$$G(t,\tau)=A\ \sin[\bar{\omega}_0\,(t-\tau)]\ \{1-\exp[-\gamma(t-\tau)]\}\ \exp[-\beta(t-\tau)] \tag{20}$$

resulted in a much better fit as can be seen in figure 5. No attempt has been made to adjust the constants, β and γ to produce an optimum fit. In fact, it may not be possible to achieve a perfect fit to the data since the driving wave, $f(t)$, used in the simulation consisted of a single cycle sine wave with an angular frequency, $2\omega_0$, twice that of the detector. This idealized waveform for $f(t)$ is only an approximation to the actual pressure waveform as shown in figure 1 (fast relaxation case). The actual detector impulse response function may also contain minor contributions at frequencies other than ω_0 which are not considered here. Approximate values obtained for the parameters in eq (20) are listed in the caption of figure 5.

The following two speculative interpretations of the functional form of eq (20) are given: 1) the circuit contains an RC of about 60 μs (value of τ in caption of fig. 5), or 2) an initially excited microphone vibrational mode transfers energy to a second mode for which the microphone exhibits a greater response. Both explanations can account for the slowly developing signal as represented by the $\{1-\exp[-\gamma(t-\tau)]\}$ term in eq (20).

We now consider how the microphone parameters change with variation of bath gas pressure and also laser intensity.

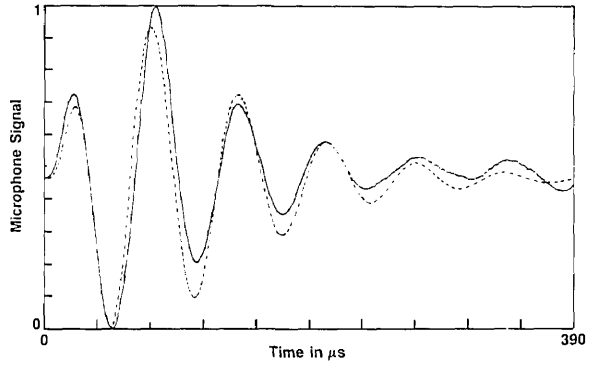

Figure 5. Solid (appearing) line is experimental microphone signal, 780 digitized data point, for a 4.7/1000 mixture of PFB in argon at a total pressure of 20 torr, time base extends from 0 to 390 μs. Dashed curve is a numerical calculation of $X(t)$ using eq (2) for the function $G(t)=A\ \sin(\omega_0 t)\cdot[1-\exp(-\gamma t)]\cdot\exp(-\beta t)$, where A is arbitrary, $\omega_0=0.097\ (\mu s)^{-1}$, $\gamma=0.017\ (\mu s)^{-1}$, $\beta=0.014\ (\mu s)^{-1}$, and the function $f(t)$ is taken as one cycle of a sine wave with an angular frequency of $2\omega_0$ and arbitrary amplitude.

4.2 Microphone Response to Laser Intensity

At a fixed total pressure, for a particular mixture, the laser light intensity was varied by a factor of about 100. This was effected by placing partially absorbing CaF_2 windows in front of the laser beam incident on the spherical chamber containing the absorbing gas and microphone. Each window was expected (from previous calibrations) to attenuate the laser beam by 65 percent. Figure 6 displays results of the microphone signal, measured at the first maximum, as a function of a number of windows placed in the path of the laser.

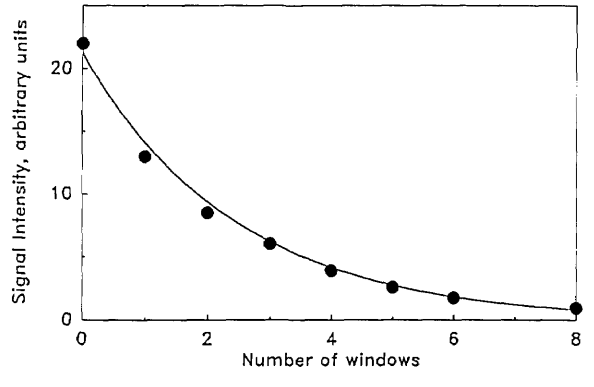

Figure 6. Relative intensity (of the first positive peak of the microphone signal) as a function of the number of attenuating BaF_2 windows.

The functional form which best fits the observed relative intensity is given by

$$I=I_0\,(0.663)^n, \tag{21}$$

where I_0 is the incident laser intensity and I is the intensity after attenuation by n windows. The addition of a single window reduces the intensity by a factor of 0.663. Since the experiments are all at a constant pressure we expect that the microphone impulse function is strictly constant, and the pressure wave impinging on the microphone also has a constant waveform. Because of the latter two conditions it is necessary that the microphone produce a signal with a constant shape (waveform), regardless of magnitude. This allows us to use any part of the resultant waveform (for example, the first maximum) as a suitable measure of the laser intensity impinging on the gas mixture. In fact, a careful review of the resultant waveforms showed that the scaled waveforms could always be precisely superposed for a two orders of magnitude change in the laser intensity. The good fit of the data to the functional form of eq (21) provides equivalent information. Figure 6 further verifies that the detector is linear over the range of excitation. Our experience has shown that pressure waves too intense can cause non-linearities in either the microphone or the amplifier or both.

4.3 Fast Relaxation: Effect of Pressure on Microphone

Experiments were performed by adding additional argon to a starting mixture of about 1/1000 PFB in argon. The starting pressure was chosen high enough (20 torr) so that energy relaxation was very fast as determined from previous measurements [11]. From a pressure of 20 torr and higher, the pressure waveform, $f(t)$, is unchanged. Assuming that the microphone impulse function, $G(t)$, is also constant, the signal waveform must also remain unchanged. We measure the amplitude of the microphone signal at several convenient points (the first maximum, for example) and plot these in figure 7 as a function of the gas pressure. Clearly, the amplitudes are not constant showing that the functional form of $G(t)$ does indeed vary with pressure. We suggest that this comes about because the damping constant, β [eq (20)] changes with pressure. On this basis the functional dependence of $G(t)$ with pressure is obtained and given in the caption of figure 7.

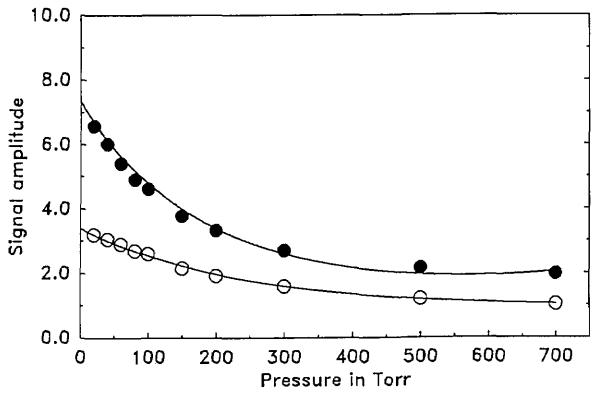

Figure 7. Pressure effect on microphone response: Amplitude (arbitrary units) of microphone signal sampled at two time points (t_0) vs total gas pressure. First pressure consists of a 20 torr mixture of 5/1000 PFB in argon. Additional pressures obtained through consecutive additions of pure argon. Open circles (sampled at $t_0=26.51\ \mu s$) fit to the expression $I=I_0 \exp[-(1.18\times10^{-4}P-0.78\times10^{-7}P^2)\cdot t]$, solid circles (sampled at $t_0=38.34\ \mu s$) fit to the expression $I=I_0 \exp[-(1.22\times10^{-4}P-1.07\times10^{-7}P^2)\cdot t]$, with time, t, in μs, the pressure, P, in torr, I_0 the amplitude extrapolated to $P=0$, and I the amplitude at pressure P.

It is interesting to see from figure 7 that the signal decay is not a linear function of pressure. There are, in fact, at least two decay rates, one considerably faster than the other, suggesting at least two microphone characteristic frequencies. We tentatively describe the fast decay to energy dissipation from a higher frequency mode of the microphone and the slow decay from a lower frequency mode. We cannot at this time quantitatively assess pressure changes in γ [eq (20)] and for present purposes assume it to be a constant.

The analysis of our experiments would be simplified if $G(t)$ were constant with pressure. Since this is not the case, the data of figures 5 and 7 allow us to arrive at $G(t)$ as a function of pressure through the use of eq (20) and the following derived parameters

$$\omega_0=0.097\ (\mu s)^{-1},\ \gamma=0.017\ (\mu s)^{-1}$$

$$\beta=(0.01+1.2\times10^{-4}P-1.0\times10^{-7}P^2)(\mu s)^{-1}, \quad (20a)$$

where the unit of time in eq (20a) is μs and the pressure P is in torr.

4.4 Analysis of Simulated Data

Before analyzing laboratory data we describe simulated experiments in which the computer algorithm, described above, numerically calculates the convolution given by eq (2). The algorithm also numerically calculates Laplace and Fourier transforms of $X(t)$, $G(t)$ and $f(t)$ performed at a single frequency, α or ω. Equations (6) and (18) were shown to be valid for a wide variety of arbitrary pressure waveforms as well as values for the parameters α and ω. That is, the transform of the "signal" was found to be equal to the product of the transform of the "pressure pulse" and the transform of $G(t)$ as expected.

Using the above computer algorithm we were in a position to evaluate the effect of "noise" on the results of data transformed at a single frequency. Thus, we performed simulations in which random as well as systematic "noise" was added to the "signal data" to determine the effect on its transform. From these limited simulations we found (qualitatively) that introduction of systematic noise in the form of baseline shifts (which we have observed experimentally to be caused by stray electrostatic signals from the laser) as well as random noise gave results in poor agreement for the Laplace transform and in good agreement for the Fourier transform as compared with the respective noise-free results.

4.5 Analysis of Relaxation Data

In agreement with the above simulations we found that the experimental data transformed using the Laplace method were considerably more scattered than data using the Fourier analogue. Typical Fourier data transforms as a function of bath gas pressure are given in figure 8. By contrast, because of the poor quality of the Laplace results, we did not analyse the data by that method. However, we should point out that base line shifts in our data which we have shown to yield poor results by the Laplace method can in principle be subtracted out. This was not attempted here; however, doing so in the future may permit more effective use of the Laplace method.

We now describe the analysis of the data of figure 8 in order to obtain the rate constant for vibrational relaxation of PFB in argon. As expected, we found that the Fourier transform returns the largest numerical value when the transform is performed at ω_0 and the results of figure 8 were so obtained. However, performing the transform at other frequencies is also possible.

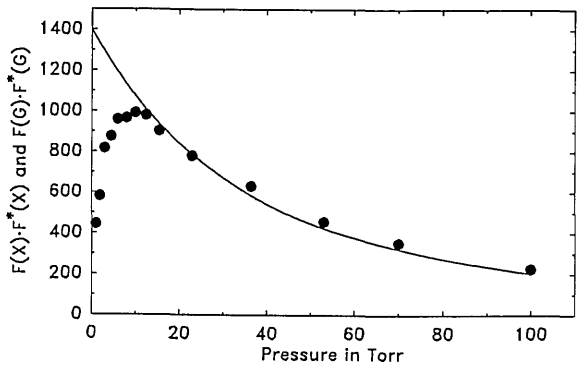

Figure 8. Data, $X(t)$ transformed according to eq (18) and presented as the solid points. The similar transform of $G(t)$ is calculated from eq (20) using the parameters listed in eq (20a). The results are displayed using the solid line.

For these experiments the laser beam dimension r_0 was set at 0.42 cm. The value for c_0, the sound velocity in argon, is 3.216×10^4 cm/s, and the frequency used for the transform, ω, is 0.097 $(\mu s)^{-1}$. These values result in $\bar{\omega}=1.256$, chosen to correspond to the simple exponential calibration curve in figure 3 ($\bar{a}=0.46$). The experimental data, $X(t)$ were transformed according to eq (18) and are presented as points in figure 8. Data up to about 20 torr mainly show the effect of vibrational relaxation while data at higher pressures show predominantly variation of the microphone's impulse response function, $G(t)$, with pressure. While pressure data as presented in figure 7, on cursory examination, suggest a moderate change of the function $G(t)$, it is seen that the operation $F(G)\cdot F^*(G)$ produces a much larger variation. However, eq (18) is entirely rigorous and is capable of handling variations in $G(t)$ and $F(G)\cdot F^*(G)$ as long as they can be quantitatively described.

There are two ways to characterize the variation of $G(t)$ with pressure. The simplest procedure is to curve fit the transformed high pressure data in figure 8 and then assume that a short extrapolation to the low pressure regime gives the proper transform of $G(t)$. Instead, we calculated $F(G)\cdot F^*(G)$ from eqs (20) and (20a), resulting in the solid line of figure 8 [12]. This calculated curve fits the experimental points reasonably well at high pressures (where it should fit the data), and serves as a means for calculating $F(G)\cdot F^*(G)$ for the low pressure points with an accuracy quite adequate for our purposes.

Finally, according to eq (18), dividing $F(X)\cdot F^*(X)$ obtained at each pressure by the calculated $F(G)\cdot F^*(G)$ at that pressure yields $F(f)\cdot F^*(f)$, the quantity of interest. The resultant curve is presented in figure 9 where the data are fit to the functional form of eq (12) (replacing the 0.75 power by unity, for this case). The best fit yields for the parameter, A, the value, 0.25. According to eq (14) (again replacing 0.75 by unity) and using for $\bar{a}$ the value 0.46 results in $\bar{k}'=0.54$. From eq (16), using $r_0=0.40$ cm and $c_0=3.078\times10^{-2}$ cm/μs, we derive $k=0.042$ $(\mu s\cdot torr)^{-1}$. This value is in good agreement with $k'=0.0428\pm0.0092$ $(\mu s\cdot torr)^{-1}$ and $k'=0.053\pm0.014$ $(\mu s\cdot torr)^{-1}$ obtained from a previous study employing two different methods [13].

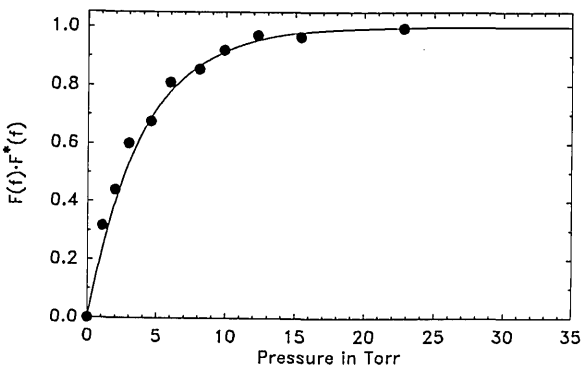

Figure 9. Each transformed data point at a given pressure (from fig. 8) divided by the transform of $G(t)$ at the corresponding pressure (taken from the solid curve of fig. 8) yields, according to eq (18), the quantity of interest, $F(f)\cdot F^*(f)$, and is presented as a solid point in this figure. These values, as a function of pressure, are best fit to the eq $F(f)\cdot F^*(f)=1-\exp(-0.25\cdot P)$, shown as the solid line.

4.6 Amplitude Method

For comparison, the amplitude of the first maximum of the microphone signal was plotted as a function of pressure in figure 10 and the functional form $[1-\exp(-0.4P^{0.75})]$ was found to be a good fit to the data. The scatter in this data is somewhat greater than in the transformed data presented in figure 8. It is interesting that the amplitude plot of figure 10 is so similar to the plot of figure 9. There is nothing in the treatment presented above that would suggest that the amplitude method should give results roughly equivalent to those obtained from the transform method.

The experimental observation that amplitude data can be used in an alternative method to derive rate constants suggests that changes in the pressure pulse waveform have perhaps less influence on the overall microphone response than changes in the magnitude of the pressure pulse, at least for the

present experimental conditions. In fact, we do observe that the microphone signal waveforms do not change markedly, particularly around the first maximum [14]. However, if the amplitude method is used, then the calibration constant, $\bar{a}$ in eq (14), must be derived through separate means, i.e., $\bar{a}$ cannot be obtained absolutely. That need not necessarily be a limitation if calibrations can be developed from mixtures possessing known relaxation rate constants or if the method described in the previous section provides the absolute standard. The amplitude method is simple and could be quite useful and worthy of further investigation.

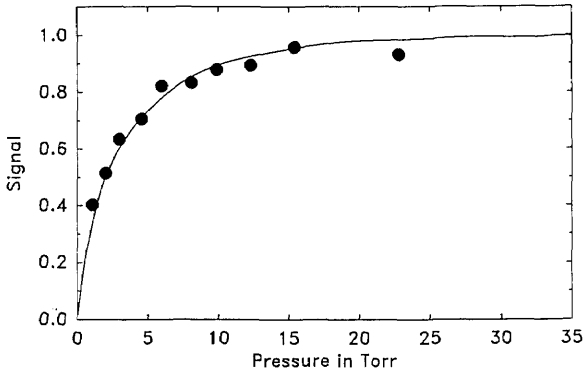

Figure 10. Amplitude data: Plot of the first positive peak of the microphone signal as a function of pressure (low pressure domain). Solid line is a fit of the data to the functional form, Signal$=1-\exp(-A \cdot P^{0.75})$, where $A=0.40$.

5. Concluding Remarks

The method requires few assumptions; these can be directly examined or verified through the use of independent methods. The assumptions include: i), the function $G(t)$ exists and ii), the signal can be represented by the simple convolution of $G(t)$ by $f(t)$ when terms involving the signal and its derivative at $t=0$ are equal to zero; iii), the variation of $G(t)$ (or its transform) with pressure can be properly dealt with; and finally, iv), the representation of $f(t)$ suitably describes the relaxation-induced pressure pulse. Assumptions i-ii have been evaluated experimentally and found to be valid; assumption iii can result in an additional source of uncertainty in the kinetic analysis if the variation of $G(t)$ through the use of an extrapolation procedure or the use of an analytic expression is inaccurate. Other detectors may show less variation of $G(t)$ with pressure and we plan to examine a number of these. Assumption iv can be assessed independently. For example, the functional form of $f(t)$ has been investigated in detail by Beck and Gordon [15] and found to be an excellent representation of the experimentally derived pressure pulse. In the derivation of $f(t)$ the additional assumption was made that first order relaxation kinetics apply. The adequacy of this assumption has been independently demonstrated for certain systems [16]. It can always be checked by simply performing kinetic measurements as a function of varying energy fluence and demonstrating the constancy of the derived "rate constant."

In the present work we employed the Fourier transform method using a single frequency coincident with the characteristic frequency of the detector. Analysis at other frequencies are of course possible and the quality of the results obtained as a function of frequency should be addressed in more detail in future work. Additionally we plan to use the Laplace transform method in experiments that are more noise-free.

The kinetic application presented here involves the measurement of the rate of energy transfer. There are other kinetic measurements which use optoacoustic detection and involve chemical reactions. Such reactions usually generate heat and the rate of heat liberation is a measure of the rate of reaction. Recently a number of such studies have been described in the literature [4,17,18]. So far they have dealt entirely with the characterization of the extent of reaction through a procedure involving amplitude analysis which has been aptly termed photoacoustic calorimetry. The method presented here should be of value to this important new area of research since it could provide the means of performing a temporal analysis from which reaction rate constants could be derived. A microphone exhibiting very high sensitivity such as the one used here would be required. We anticipate initiating experiments of this kind.

About the authors: All the authors are in the NIST National Measurement Laboratory. Walter Braun is with the Chemical Kinetics Division, Philippe Dagaut is a guest worker in the Chemical Kinetics Division, and Barry C. Cadoff is with the Gas and Particulate Science Division.

6. References

[1] Smith, N. J. G., Davis, C. C., and Smith, I. W. M., J. Chem. Phys. **80**, 6122 (1984).

[2] Beck, K. M., Ringwelski, A., and Gordon, R. J., Chem. Phys. Lett. **121**, 529 (1985).

[3] In order to simplify the discussion in the present paper we (somewhat unconventionally) refer to waveform or wave shape as being synonymous and distinct from intensity, or its equivalents, magnitude or amplitude. The latter term or terms, viewed as a scaling factor, convert each infinitesimal segment of a given waveform into an equivalent waveform segment of proportionally greater or lesser magnitude.
[4] Rothberg, L. J., Simon, J. D., Bernstein, M., and Peters, K. S., J. Amer. Chem. Soc. **105**, 3464 (1983).
[5] Kreuzer, L. B., J. Appl. Phys. **42**, 2934 (1971).
[6] Greenberg, M. D., Application of Green's Functions in Science and Engineering, Prentice-Hall, Inc., Englewood Cliffs, NJ (1971).
[7] The transform of a function, $F(t)$ is defined as $L[F(t)]=\int_0^\infty \exp(-st)\cdot F(t)\cdot dt=f(s)$. We define a single-frequency transform as, $L[F(t)]s_0=\int_0^\infty \exp(-s_0t)\cdot F(t)\cdot dt=f(s_0)$, that is the value returned by the specified operation using a fixed value of s, namely s_0. For the sake of clarity we identify the use of a single-frequency transform using the former notation and by specifying the positive, real number, s_0, by the symbol α. The symbol ω will subsequently be reserved for the case of the Fourier transform obtained at the fixed frequency, ω.
[8] Bailey, R. T., Cruickshank, F. R., Guthrie, R., Pugh, D., and Weir, I. J. M., Mol. Phys. **48**, 81 (1983).
[9] Two independent studies have shown that "tophat" rather than Gaussian geometry best describes IR laser irradiation; Beck, K. M., and Gordon, R. J., J. Chem. Phys. **87**, 5681 (1987); and Braun, W., Wallington, T. J., and Cvetanovic, R. J., J. Photochem. Photobiol., A: Chemistry **42**, 207 (1988).
[10] Certain commercial equipment and instruments are identified in this article in order to adequately specify the experiments described here. Such identification does not imply recognition or endorsement by the National Institute of Standards and Technology, nor does it imply that the material or equipment identified are necessarily the best available for the purpose.
[11] Wallington, T. J., Scheer, M. D., and Braun, W., Chem. Phys. Lett. **138**, 538 (1987).
[12] It should be mentioned that while pressure changes can cause a variation in the microphone impulse response function, $G(t)$, it can also cause a variation in the energy/pressure derived from the laser beam. Since the latter entirely produces an amplitude effect it is properly accounted for by means of the procedure(s) described here.
[13] Wallington, T. J., Braun, W., Beck, K. M., and Gordon, R. J., J. Phys. Chem. **92**, 3839 (1988).
[14] A similar observation was made by Barker, J. R., Brouwer, L., Patrick, R., Rossi, J. J., Trevor, P. L., and Golden, D. M., Int. J. Chem. Kinet. **17**, 991 (1985).
[15] See reference cited in reference [9].
[16] Braun, W., and Wallington, T. J., Chem. Phys. Lett. **140**, 441 (1987).
[17] See reference [14].
[18] Anderson, V. E., Cheng, H. Z., Diebold, G. J., Mahmood, A., and Sweigart, D. A., J. Amer. Chem. Soc. **109**, 6191 (1987).

Volume 93, Number 6, November–December 1988
Journal of Research of the National Institute of Standards and Technology

Solvent-Free Injection in Supercritical Fluid Chromatography Using Sintered Glass Deposition

Volume 93 Number 6 November–December 1988

Thomas J. Bruno

National Institute of Standards and Technology
Boulder, CO 80303

Sample injection in supercritical fluid chromatography (SFC) is usually performed using a combination of apparatus from liquid chromatography and capillary gas chromatography. The device most often consists of an injection valve (of the type used in liquid chromatography) followed by a flow splitter controlled by a restrictor. It is sometimes desirable to inject samples in the absence of a solvent, as in physicochemical applications of SFC. In this article, two simple modifications to a conventional sampling valve system are presented which allow solvent-free injection. Using these devices, sample (in a solvent) is deposited on a sintered glass bed. After removal of the solvent by mild heating and evacuation, the sample loop is filled with the supercritical carrier and the valve is switched to the inject position.

Key words: chromatography; injection; supercritical fluid chromatography; supercritical fluids.

Accepted: July 27, 1988

Sample introduction in analytical applications of supercritical fluid chromatography (SFC) is usually performed using a high-pressure multiport sampling valve (of the type used for high-performance liquid chromatography—HPLC) equipped with a flow splitter. The splitter is most often of fixed split ratio (for a given pressure and temperature): the ratio is determined and controlled by a fused silica capillary restrictor. The sample, which is usually a solid or liquid dissolved in an appropriate solvent, is syringe loaded into the sample loop of the multiport valve, and injection is achieved by switching the position of the valve. The solvent will be separated from the sample species by the physical and chemical interactions with the stationary phase in the column.

In some nonanalytical applications of supercritical fluid chromatography it is often desirable to inject a sample (which may be of low volatility) in the absence of solvent. Such applications are typically in physicochemical measurement studies. As an example, we may consider the chromatographic determination of binary diffusion coefficients using the Taylor-Aris method [1–5]. In this technique, a sample is injected onto the head of an open tubular column as a sharply defined spike. As the carrier moves the sample through the length of the tube, the initial sharply defined spike will broaden into a Gaussian-like profile. For this experiment, the column is uncoated and ideally should be inert, and the presence of a solvent would ruin the measurement.

In order to allow convenient injection of relatively nonvolatile solutes for this type of measurement, we have used two approaches to provide a solvent-free injection. In the first approach, a standard multiport injection valve has been modified to accept the deposition of sample on a small section of sintered glass placed within the sample loop. In the second approach, an extractor based on sintered glass deposition precedes the sampling valve. Sintered glass was chosen as the deposition

material for several reasons. First, since glass has a relatively high energy surface, one would expect a conveniently-sized aliquot of sample to be easily loaded. In addition, there is no danger of the sintered glass bed being displaced from its position in the loop or extractor. An initial series of devices packed with small beds of chromatographic supports (such as Tenax-GC[1]) was unsatisfactory for this reason.

In the first approach, the sample loop is fitted with a nichrome heater wire, and the valve block with a cartridge heater to provide temperature control. A schematic diagram of the modified sample loop is provided in figure 1. The sintered glass, which was obtained from a commercial supplier as a 0.16-cm (0.0625-in) thick disk, was cut into cylindrical sections (of 0.16-cm diameter) using a core drill. To fabricate a loop, one or more of these wafers are interposed in the center of a sample loop [consisting of 316 stainless steel tubing of 0.02-cm (0.009-in) inside diameter and 0.16-cm (0.0625-in) outside diameter] constrained by a small stainless steel cylinder [0.32-cm (0.125-in) outside diameter and 0.16-cm (0.0625-in) inside diameter]. This outer cylinder is brazed to the sample loop using a hydrogen torch. A hydrogen torch was employed to avoid using flux, which could contaminate the sintered glass bed. The sampling loop thus modified is then installed as part of a high-pressure analogue of a sampling system described previously [6]. This sampling system contains provisions for pressurization, venting, and evacuation of the sample loop. The high-pressure limit of this sample loop is constrained by that of the sampling valve [approximately 41 MPa (6000 psi)]. Calculations indicate, however, that the maximum allowable working pressure of the modified loop itself is in excess of 96 MPa (approximately 14,000 psi).

The use of this sampling device is quite simple. A solvent-borne solute is loaded via syringe into the sampling loop as one would in HPLC. In this case, the more volatile the solvent and the less volatile the solute, the better. The sample loop and valve are then warmed and the solvent vapors vented. The loop is then evacuated to remove as much residual solvent vapor as possible. Naturally, the longer the evacuation time, the more solvent will be removed. A heating-evacuation cycle of between 5 and 7 min is usually sufficient to remove all but trace quantities of most common solvents.

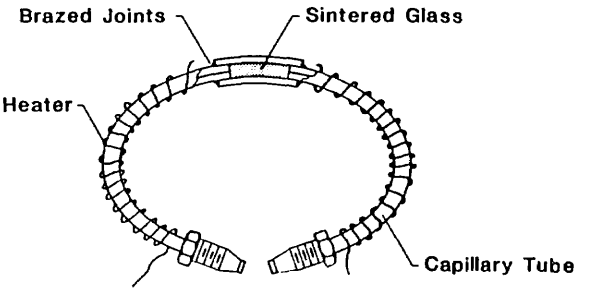

Figure 1. A schematic diagram of the modified sample loop containing a cylinder of sintered glass.

The chromatogram presented in figure 2 was obtained using this sampling technique in a developmental supercritical fluid chromatograph designed and built for physicochemical measurements. The sample in this case was a 0.01 percent (mass/mass) solution of naphthalene in methylene chloride. The solution was loaded into the loop using an HPLC syringe, and the methylene chloride solvent was removed by a heating-evacuation cycle (at a temperature of approximately 50 °C for 5 min). The loop was then pressurized with carbon dioxide at 13.8 MPa (2000 psi), with the loop and sampling valve being held at 50 °C. An equilibration time of approximately 1 min was allowed for the dissolution of the naphthalene in the carbon dioxide.

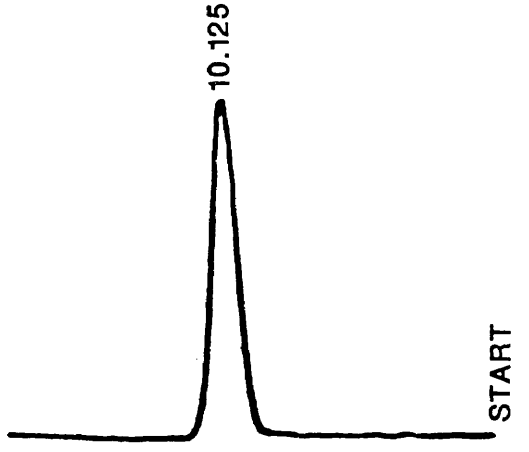

Figure 2. A chromatogram showing the FID response of naphthalene in supercritical carbon dioxide at 20.7 MPa (3000 psi) and 130 °C. The electrometer was set at a range of 10^{-11}, with attenuation of 1.

[1] Certain commercial equipment, instruments, or materials are identified in this paper in order to adequately specify the experimental procedure. Such identification does not imply recommendation or endorsement by the National Institute of Standards and Technology, nor does it imply that the materials or equipment identified are necessarily the best available for the purpose.

Switching of the sampling valve then resulted in the injection into the carrier stream at a pressure of 20.7 MPa (3000 psi) and 130 °C (the conditions of the chromatographic experiment). The pressurization step described above is done at a pressure lower than the column initial pressure so as to counteract somewhat the deleterious effect of the relatively large volume of the modified loop. In the case of figure 2, the column was a 3050-cm uncoated stainless steel tube [0.23-cm (0.009-in) inside diameter], and detection was done using a modified flame ionization detector [7]. The symmetry of the peak is indicative of negligible adsorptive interference by the sintered glass bed.

There are a number of advantages associated with this method of injection. The first is, of course, the removal of the solvent when solvent-free injection is required. In addition, there is a greatly reduced need to use a flow splitter since most of the applied sample is solvent, which is removed during the heating-evacuation step. To reduce the amount of solute injected, one simply dilutes the solution applied to the sintered glass. The solute is then actually injected in a solution of the supercritical carrier. The major disadvantage experienced with the technique is the relatively long time involved in completing an injection (approximately 8 min). Improvements along these lines are currently being pursued. Since another disadvantage is the relatively large loop volume, attempts are being made to minimize the size of the sintered glass bed. The problems caused by large loop volume (such as peak broadening and pressure pulsation) appear to be relatively minor, however, as judged from comparative HETP (height equivalent to a theoretical plate) determinations.

A second approach we have had success with makes use of a small extractor placed ahead of the sampling valve. This approach is similar to that taken by others in physicochemical measurements [8,9]. The extractor is shown schematically in figure 3. The manifold arrangement used with this extractor is shown in figure 4. The extractor itself was machined from a section of 316 stainless steel bar, 12.7 cm in diameter and 4 cm in length. A hole (0.32-cm diameter) bored through the center of the bar accommodates a section of cut sintered glass, as in the sample loop approach described earlier. The extractor is sealed at either end using threaded or brazed fittings. A syringe loading tube is brazed onto the side of the extractor body, and is capped using a compression fitting plug.

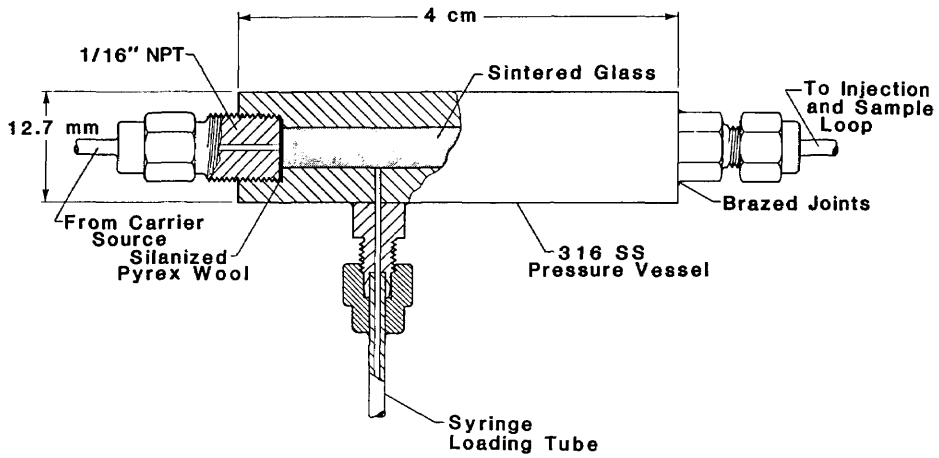

Figure 3. A schematic diagram of the extractor (which precedes the sampling valve). The manifold for this extractor is shown in figure 4.

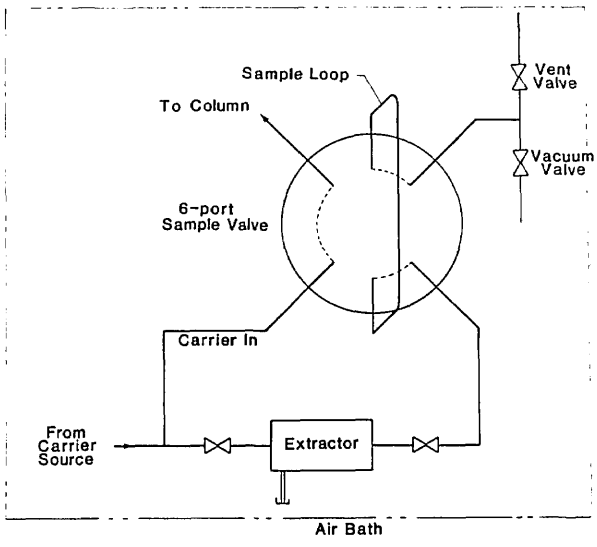

Figure 4. A schematic diagram of the manifold which controls the extractor (which is shown in fig. 3). The sampling valve is shown in the "fill" position.

To use this extractor, a solvent-borne sample is loaded onto the sintered glass bed through the loading tube using a conveniently-sized syringe. After capping the loading tube with a pressure fitting (not shown in fig. 3), the extractor and transfer lines are evacuated using the vacuum valve. Solvent evaporation is aided by raising the temperature of the entire manifold, which is contained in an air bath. The extractor is then filled with the carrier using the inlet valve. As can be seen from figure 4, the position of the chromatographic injection valve determines if the loop is filled. Usually, the injection valve is in the inject or flow position until carrier and sample have had time to equilibrate. After the sampling valve is switched to the inject position, the inlet valve may be reopened to insure that the carrier pressure will be the same in both the chromatographic column and the sampling loop. The density will also depend upon the temperature, thus to achieve density equivalence, the chromatographic column and injection manifold must be at the same temperature. This generally will pose no difficulty, since one sample loading can usually provide enough solute for dozens of injections.

Acknowledgment

The financial support of the United States Department of Energy, Office of Basic Energy Sciences, is gratefully acknowledged.

About the author: Thomas J. Bruno is a physical chemist in the Thermophysics Division of the National Engineering Laboratory at the National Institute of Standards and Technology, Boulder, CO.

References

[1] Conder, J. R., and Young, C. L., Physicochemical Measurement by Gas Chromatography, John Wiley and Sons, Chichester (1979).
[2] Laub, R. J., and Pecsok, R. L., Physicochemical Applications of Gas Chromatography, John Wiley and Sons, New York (1978).
[3] Taylor, G. I., Proc. Roy Soc. (London), Ser. A **219**, 186 (1953).
[4] Taylor, G. I., Proc. Roy Soc., Ser. A **225**, 473 (1954).
[5] Aris, R., Proc. Roy. Soc., Ser. A **235**, 67 (1956).
[6] Bruno, T. J., J. Chromatogr. Sci. **23**, 325 (1985).
[7] Bruno, T. J., Proc. Fifth Symp. Energy Eng. Sci. (CONF-8706187) Argonne, IL (1987) pp. 52–60.
[8] Smith, R. D., Udseth, H. R., Wright, R. W., and Yonker, C. R., Sep. Sci. Tech. **22**, 1065 (1987).
[9] Roth, M., Steger, J. L., and Novotny, M. V., J. Phys. Chem. **91**, 1645 (1987).

Volume 93, Number 6, November–December 1988
Journal of Research of the National Institute of Standards and Technology

Paper from the Accuracy in Trace Analysis Symposium Proceedings not included in J. Res. Natl. Bur. Stand., Vol. 93, No. 3 (1988)

Enzyme-Enhanced Electrochemical Immunoassay for Phenytoin

Mirtha Umaña, Jess Waller, Mansukh Wani, Carol Whisnant, and Edgar Cook

Research Triangle Institute
Post Office Box 12194
Research Triangle Park, NC 27709-2194

Introduction

The use of electrochemically generated electron-transfer mediators to control the oxidation states of enzymes has been the subject of considerable research [1,2]. Among these studies, the oxidation of glucose by glucose oxidase (GOx) has been extensively studied. Ferrocene derivatives [3] and other redox compounds [4,5] have been used to mediate the oxidation of dissolved and immobilized GOx [6]. Polypyrrole has been used to immobilize GOx on the surface of electrodes [7,8,9]. This polymer provides a simple and effective immobilization medium, and because it is an electronic conductor, it is expected to facilitate the electron transfer to the enzyme.

An important application of enzyme-mediated electrocatalysis is in immunoassays where the current amplification of the enzyme reaction enhances the sensitivity of the measurement. The immunological utility of the ferrocene/GOx system has been demonstrated with lidocaine as the antigen [10]. The general scheme is illustrated in figure 1; ferrocene-antigen (Fer-Ag) is competitively displaced from the antibody (Ab) by Ag, the analyte, and it is determined as an enzyme-amplified oxidation current. This scheme has significance because it expands the applicability of electrocatalytic analysis to analytes currently determined by immunoassays, and thus, deserves further research to demonstrate its generality.

This paper describes experiments aimed at understanding the kinetics and mechanism of the reaction, at determining the optimum conditions for the assay, and at testing the generality of the scheme shown in figure 1. We have chosen phenytoin [5,5-diphenylhydantoin (DPH)] as the model antigen, because of its clinical importance. For this drug to be effective and safe, plasma levels must be between 5 and 20 mg/L [11]. Thus, the development of easy, real-time assays for this and other critical-level drugs is highly desirable.

This paper also describes preliminary results on the electron-transfer mediation of ferrocene derivatives to polypyrrole-immobilized GOx. The goal of these experiments is to couple the polypyrrole-immobilized GOx to the ferrocene-DPH system to produce a reagentless electrochemical immunoassay sensor, so that easy, real-time determinations may be realized.

Experimental

Electroanalysis was conducted with a PAR 175/173 potentiostat, in a three-electrode assembly (GC, Ag/AgCl, Pt). A two-compartment cell was used for immunological experiments. Preparation and use of GOx-polypyrrole modified electrodes (GOx/PP/GC) have been described elsewhere [7,8]. The polyclonal anti-DPH serum was prepared at RTI [12].

Ferrocene-phenytoin (Fer-DPH) was synthesized inhouse. To a room-temperature stirred solution of ferrocene carboxylic acid and 3-(2-aminoethyl)-5,5-diphenylhydantoin in anhydrous THF, 1,3-dicyclohexylcarbodiimide was added in one portion. After 5 h, the solvent was removed in vacuo. The residue was purified by elution from silica gel (5 g) using 20% acetone in hexane to yield a yellow solid with m.p. 248–251 °C. NMR, high resolution mass spectrometry, and elemental analysis confirmed the identity of the compound. Fer-DPH is insoluble in water but soluble in 10% CH_3CN. Typical cyclic voltammograms (CVs) of DPH-Fer conjugate produced $E^{\circ\prime}=0.47$ V vs Ag/AgCl and 0.06 V peak separation.

Results and Discussion

The DPH antibody binding was compared to that of Fer-DPH in a competitive inhibition RIA using ^{3}H-DPH (specific activity 40.3 Ci/mmol/L) as tracer. Anti-DPH antibodies (DPH affinity $>10^9$ L/mol) showed 25% cross-reactivity (at 50% displacement of radioligand) with Fer-DPH. Thus, the Ab binding to Fer-DPH is sufficiently strong to

Volume 93, Number 6, November-December 1988
Journal of Research of the National Institute of Standards and Technology

Paper from the Accuracy in Trace Analysis Symposium Proceedings not included in J. Res. Natl. Bur. Stand., Vol. 93, No. 3 (1988)

form a stable Fer-DPH-Ab complex but DPH will readily displace Fer-DPH as needed for the scheme shown in figure 1.

The CVs of Fer-DPH are completely quenched by the formation of Fer-DPH-Ab upon addition of 100 μL DPH antiserum. The inability of Fer-DPH-Ab to exchange electrons with the electrode may be due to steric effects, since the antibody may block the redox center from the electrode.

Kinetic information on the electrocatalysis was obtained with scan rate dependence studies. In the absence of GOx, the current (i_d) is determined by diffusion of the ferrocene derivative and is expected to obey the Randles-Sevcik relationship for a reversible system:

$$i_d = 2.69 \times 10^5 \, n^{3/2} A \, D^{1/2} \, C_0^* \, \nu^{1/2}, \quad (1)$$

where n is the number of electrons, A is the area of the electrode, D is the diffusion coefficient, C_0^* is the concentration of electroactive species in the solution, and ν is the scan rate.

In the presence of GOx and excess glucose, the limiting value of the current response (i_k) is independent of ν:

$$i_k = n F A \, C_0^* \, (D \, k' \, C_z^*)^{1/2}, \quad (2)$$

where F is the Faraday constant; C_z^* is the enzyme concentration, and k' is the rate constant for the catalytic reaction. From scan rate dependence studies [13], we estimated a pseudo first-order rate constant for the catalytic reaction of GOx with ferrocene carboxylic acid and Fer-DPH of approximately 2×10^5 and 4×10^5 $mol^{-1}L^{-1}$, respectively. These values are comparable to the ones previously reported for ferrocene derivatives [5]. In the presence of 1.5 mmol/L GOx, the catalytic current is about three times the Fer-DPH background current and increases with enzyme concentration but is independent of glucose (above 20 mmol/L). Thus, the overall current is governed by the rate of reaction of the ferrocene with GOx rather than the rate of reaction of GOx with glucose as needed for the scheme of figure 1.

Experiments shown in figure 2 demonstrate the development of the DPH electrochemical immunoassay. The CV of Fer-DPH is observed in curve a; upon addition of GOx and glucose, a large catalytic current is observed in curve b; upon addition of DPH-antiserum the catalytic current is almost completely inhibited in curve c; and after addition of DPH, due to the release of Fer-DPH from the antibody complex by the competitive binding of DPH, the catalytic current is recovered in curve d. The increase in current from curve c to curve d, is proportional to the amount of DPH added, and can be quantitated to produce a standard curve of DPH (pharmacologically relevant range) as shown in figure 3.

Currently, experiments aimed at producing a reagentless electrochemical immunoassay using a GOx/PP/GC electrode are in progress. GOx/PP/GC electrodes were examined for their response to ferrocene derivatives. The GOx/PP/GC electrodes were potentiostatted at 0.5 V, in an oxygen-free solution containing a measured amount of ferrocene. After addition of an excess of oxygen-free glucose solution, the current increased as expected from figure 1. The catalytic current increased linearly with ferrocene (10^{-4} mol/L). Extrapolation to zero ferrocene shows a current increase (5 nA) due to the addition of glucose to a solution that contained no electron-transfer mediator. An explanation for this current increase may be that electrons are transferred directly from the polypyrrole that surrounds the GOx to its active center. This hypothesis is currently under investigation by monitoring the disappearance of glucose.

Acknowledgment

We thank the Research Triangle Institute staff: E. Holt for the immunological studies and D. Rector for synthesis, and Dr. R. W. Murray of UNC for helpful discussions. This work was funded by the Army Research Office under Contract Number 85-G-05201.

Volume 93, Number 6, November–December 1988
Journal of Research of the National Institute of Standards and Technology

Paper from the Accuracy in Trace Analysis Symposium Proceedings not included in J. Res. Natl. Bur. Stand., Vol. 93, No. 3 (1988)

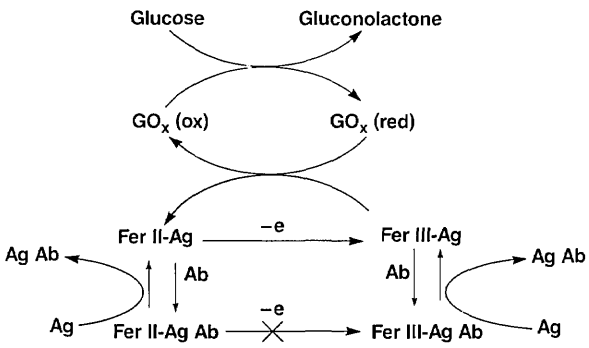

Figure 1. The catalytic cycle of GOx using ferrocene derivatives as electron-transfer mediators interrupted by the binding of an antibody to a ferrocene-antigen conjugate.

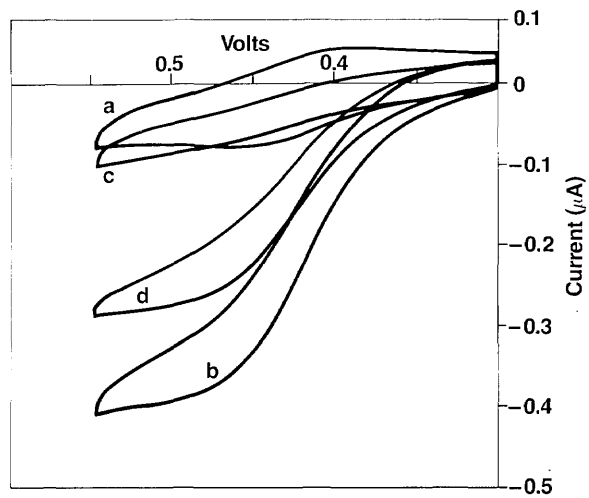

Figure 2. Cyclic voltammograms of Fer-DPH conjugate in aqueous 0.5 mol/L KCl at pH 7 with 10% CH_3CN. a) 200 mmol/L Fer-DPH, b) after addition of 40 mmol/L glucose and 0.8 mmol/L GOx, c) after addition of anti-DPH serum, d) after addition of DPH.

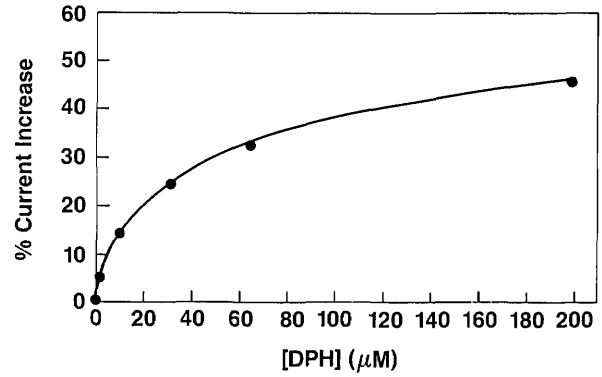

Figure 3. Calibration plot for electrochemical immunoassay of DPH.

References

[1] Schlapfer, P., Mindt, W., and Racine, Ph., Clin. Chem. Acta **57**, 283 (1974).
[2] Alecsandrovskii, Y. A., Beshikina, L. V., and Rodionov, Y. V., Biokhimiya **46**, 708 (1981).
[3] Cass, A. A. G., Davis, G., Graeme, D. F., Hill, H. A. O., Aston, W. J., Higgins, I. J., Plotkin, E. V., Scott, D. L., and Turner, A. P. F., Anal. Chem. **56**, 667 (1984).
[4] Crumliss, A. L., Hill, H. A. O., and Page, D. J., J. Electroanal. Chem. **206**, 327 (1986).
[5] Albery, W. J., Bartlett, P. M., and Cransten, D. H., J. Electroanal. Chem. **194**, 223 (1985).
[6] Lange, M. A., and Chambers, J. Q., Anal. Chim. Acta **175**, 89 (1985).
[7] Umaña, M., and Waller, J., Anal. Chem. **58**, 2979 (1986).
[8] Umaña, M., and Waller, J., Proc. of the U.S. Army CRDEC Scientific Conference on Chemical Defense Research, Vol. 2, 18–21 November 1986, p. 879.
[9] Foulds, N. C., and Lowe, C. R., J. Chem. Soc. Faraday Trans., 1259 (1986).
[10] Glerian, K. D., Hill, H. A. O., McNeil, C. J., and Green, M. J., Anal. Chem. **58**, 1203 (1986).
[11] Cook, C. E., Amerson, E., Poole, W. K., Lesser, P., and O'Tuama, L., Clin. Pharm. Therap. **18**, 742 (1975).
[12] Cook, C. E., Kepler, J. A., and Christensen, H. D., Res. Comm. Chem. Pathol. Pharmacol. **5**, 767 (1973).
[13] Nicholson, R. S., and Shain, I., Anal. Chem. **36**, 707 (1964).

Volume 93, Number 6, November–December 1988
Journal of Research of the National Institute of Standards and Technology

Paper from the Accuracy in Trace Analysis Symposium Proceedings not included in J. Res. Natl. Bur. Stand., Vol. 93, No. 3 (1988)

Liposome-Based Flow Injection Immunoassay System

Laurie Locascio-Brown, Anne L. Plant, and Richard A. Durst

Center for Analytical Chemistry
National Institute of Standards and Technology
Gaithersburg, MD 20899

The development of many biochemical assays is dependent upon the specific interaction of an antigen with its antibody. This interaction is usually monitored using secondary labels with the most popular immunoassays employing fluorescent or radioactive tracers for detection of a single binding event. We are developing a novel flow injection analysis (FIA) system which contains an immunospecific reactor column and utilizes liposomes for detection. The fluorophore-loaded liposomes used in this assay can be made to provide signal enhancement in the range of one thousand to one million times per binding event making fluorescent assays competitive in sensitivity with radioimmunoassays.

Liposomes are spherical structures composed of phospholipid bilayers that form spontaneously when phospholipid molecules are dispersed in water. The interior and exterior environments of liposomes are aqueous and, therefore, liposomes can be prepared with large numbers of water-soluble marker molecules trapped in their internal aqueous space. Liposomes are prepared by the injection method [1] from a mixture of dimyristoylphosphatidylcholine: cholesterol: dicetyl phosphate with a molar ratio of 5:4:1. Approximately 1×10^3 carboxyfluorescein molecules are encapsulated inside each liposome when the liposomes are formed in 3 mmol/L carboxyfluorescein solution. The liposomes may be "sensitized" to a particular antigen through covalent binding of that antigen to the polar head group of a phospholipid molecule which is incorporated into the lipid mixture at about 1 mol % prior to liposome formation. When the liposome is formed in water, approximately half of the antigen will be exposed to the external solution, and, therefore, will be available to interact with antibody binding sites. The combining of antigen on these "sensitized" liposomes with antibody can then be monitored through the fluorescence of the encapsulated marker molecule. In this assay, each binding event is amplified approximately 1000 times. Liposomes containing 3 mmol/L carboxyfluorescein are about 0.1 μm in diameter, and have a polydispersity of 0.1 which corresponds to a size distribution of 0.5% as determined by photon correlation spectroscopy with data analysis using the cumulants method [2]. The diffusion coefficient of these liposomes in water was determined to be 5×10^{-8} cm^2/s, and the liposomes contained 1–5 lamellae per liposome. These liposomes have been determined to be stable for greater than 3 months in TRIS buffer at room temperature.

The flow injection system contains a glass reaction column (2.0 mm i. d.$\times$99.5 mm; total volume of 155 μL) packed with nonporous glass beads 250±40 μm in diameter (60–80 mesh) which provide the solid phase for the immuno-specific reaction. The antibody is covalently bound to the solid support in a manner which ensures the proper orientation of the antibody binding site such that there is very little loss in activity. The antibody is prepared for binding by initially cleaving the Fc portion of the antibody with pepsin leaving an $F(ab')_2$ fragment attached in the hinge region through a disulfide bond. Reducing this disulfide bond yields two Fab' fragments with equal affinity for antigen binding and with a sulfhydryl group at the base of the fragment available for attachment. Covalent immobilization of this Fab' fragment is achieved through silanization of the beads with an aminosilane reagent. An amide bond is formed between the aminosilane and a difunctional succinimidyl-maleimido linking agent. The Fab' fragment is then easily attached to the maleimido group through the sulfhydryl group at the base of the antibody fragment (fig. 1). Several preparations of nonporous soda lime glass beads derivatized with a monofunctional silane have proven to be stable in a packed column for 7 d when subjected to a flow rate of 1 mL/min in slightly basic TRIS buffer. Quantitation of silanized sites is accomplished through acetylation of the amino group using ^{14}C-labeled acetic acid. Detection of the interaction between sample antigen (analyte) molecules, and the covalently immobilized antibodies is achieved by competition with liposomes that are "sensitized" with antigen.

Volume 93, Number 6, November-December 1988
Journal of Research of the National Institute of Standards and Technology

Paper from the Accuracy in Trace Analysis Symposium Proceedings not included in J. Res. Natl. Bur. Stand., Vol. 93, No. 3 (1988)

The flow properties of liposomes in flow injection systems were investigated to determine optimal conditions for competitive immunochemical binding events in a heterogeneous sample. It was found that due to the large differences in diffusion coefficients of liposomes and small solution molecules, some separation of the sample and liposome solution boluses occurred prior to the introduction of the mixture onto the column. This precolumn separation reduces the sensitivity of the assay since the arrival of the liposome bolus precedes the sample bolus, and many sites become saturated before any competition can take place. Precolumn mixing of the liposome suspension reduces the separation of the boluses, and a simple solution to the problem was found in simultaneous separate injection of the liposome-antigens and free antigens. The liposome-antigens were injected using a knitted sample loop while sample solutions were injected through a straight sample loop [3] as shown in figure 2. This manipulation was sufficient to cause significant precolumn bolus overlap, and allowed the full benefit of performing a competitive assay.

The stability of liposomes was studied when exposed to the materials and flow rates commonly used in a flow injection apparatus. Liposomes were found to be unstable when exposed to the underivatized glass bead column due to the loss of lipid from the liposome bilayer to hydrophobic sites on the column. Conditioning of the system with lipid prior to the introduction of liposomes helped to stabilize the structures by saturating any exposed hydrophobic sites. The sites remained saturated with continuous use of the system for 2 weeks due to the slow partitioning of the lipid into the aqueous phase. The liposomes were also tested under higher flow rates to determine the degree of rupturing due to shear forces. No leakage of carboxyfluorescein from the structures was observed when exposed to flow rates of 2 mL/min which is typical for use in FIA. The results obtained from injections of liposome samples after conditioning were very reproducible with consistency in dispersion and peak symmetry.

The hydrodynamic characteristics of liposomes were studied extensively to determine the feasibility of using liposomes as analytical reagents in flowing systems. Liposomes are bulky structures in a typical flow injection system with a diameter that corresponds to roughly 1/5000 of the tube diameter. The heterogeneity and the size of the liposomes in solution made it important to determine if the behavior of these structures was consistent with that predicted by the theory developed for a homogeneous solution containing molecules of a similar diffusion coefficient. In theory, the dispersion squared is linearly related to the length of straight tubing through which the sample flows. In a homogeneous solution, the slope of this plot is a constant which is inversely proportional to the square root of the diffusion coefficient. When heterogeneous mixtures are injected into a flowing stream, we can expect some partitioning of the particulates out of the flow stream resulting in uncharacterized dispersions. Plots of carboxyfluorescein-loaded liposomes and carboxyfluorescein solution behavior gave straight lines with correlation coefficients of 0.92 and 0.99, respectively. The ratio of the respective slopes is approximately equal to the inverse ratio of the square root of the diffusion coefficients suggesting that liposome behavior closely follows the behavior of a homogeneous solution. The behavior of liposomes in other common components of a flow injection system, such as a knitted delay tube and a packed reactor column, showed that liposome flow mimicked the theoretical behavior of a homogeneous solution. Therefore, liposome suspensions may be used in FIA as calibration solutions, and so are appropriate analytical reagents in methods of continuous analysis.

Volume 93, Number 6, November–December 1988
Journal of Research of the National Institute of Standards and Technology

Paper from the Accuracy in Trace Analysis Symposium Proceedings not included in J. Res. Natl. Bur. Stand., Vol. 93, No. 3 (1988)

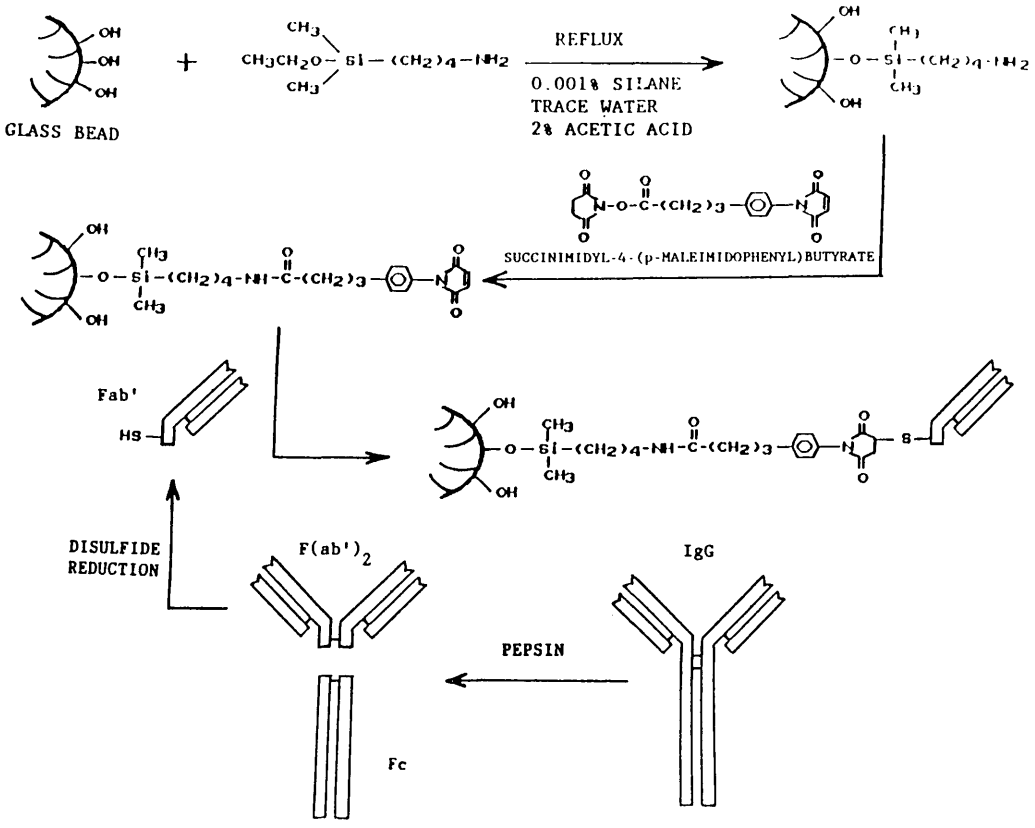

Figure 1. Silanization of nonporous glass bead surface, and covalent attachment of Fab' fragment.

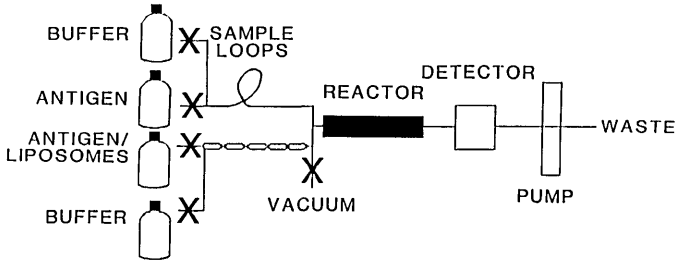

Figure 2. Flow injection system with simultaneous double injection. Xs represent microprocessor-controlled solenoid pinch valves.

References

[1] Batzri, S., and Korn, E. D., Biochim. Biophys. Acta **298**, 1015 (1973).
[2] Koppel, D. E., J. Chem. Phys. **57**, 4814 (1972).
[3] Locascio-Brown, L., Plant, A. P., and Durst, R. A., Anal. Chem. **60**, 792 (1988).

Volume 93, Number 6, November–December 1988
Journal of Research of the National Institute of Standards and Technology

Conferences/Events

WORKSHOP ON MICROSTRUCTURE AND MACROMOLECULAR RESEARCH WITH COLD NEUTRONS
National Bureau of Standards, Gaithersburg, MD, April 21–22, 1988

On April 21–22, 1988, over 160 scientists, including 25 from industry, 70 from universities and 30 from government laboratories and agencies (not including NBS), gathered at NBS, Gaithersburg, for a Workshop on Microstructure and Macromolecular Research with Cold Neutrons. This workshop was one of a series, each devoted to a major area of research with cold neutrons, that are being held in conjunction with the development of the Cold Neutron Research Facility (CNRF) at the NBS 20 MW research reactor as a national, user-oriented research facility. The dual aims of this workshop were to highlight research opportunities in the application of cold neutron techniques to the study of submicron structure in materials and macromolecular systems, and to inform and involve the scientific community in the planning for instrumentation for the CNRF.

The long wavelength neutrons that are produced by a cold moderator, such as the 40 K D_2O-ice moderator recently installed in the NBS reactor, are a powerful probe of both the structure and dynamics of materials. The emphasis of this workshop was on the structural applications of cold neutrons. Thus techniques such as small angle neutron scattering (SANS), which probes structure in bulk materials on the 1 to 100 nm scale, and the relatively new technique of neutron reflectometry, which probes near surface structure to depths of tenths of microns, were discussed in detail. For both of these techniques, cold neutrons substantially extend the distance scale probed and improve the spatial resolution beyond what has been possible with thermal neutrons.

The first morning session of the workshop on Scientific Opportunities with Cold Neutrons opened with a review by T. Russell (IBM Almaden Research Center) of the impact SANS has had on Polymer Science in general, and on the understanding of the interactions and correlations in polymer mixtures in particular. Russell also discussed recent developments, important to the development of polymer composites, in the use of grazing incidence neutron and x-ray scattering for the evaluation of conformation changes and concentration gradients in polymer mixtures near surfaces and at interfaces. The use of scattering methods to characterize such seemingly dissimilar materials as porous rock and agglomerated colloids was the subject of the talk by S. K. Sinha (Exxon Research and Engineering Co.). Sinha presented a general formalism which unified the concepts of surface and mass fractals and showed how the self-similar nature of fractal structures is most directly revealed through scattering measurements. Several examples were presented which underscored the need for scattering instruments which probe a wide range of length scales in order to accurately determine the nature and limits of fractal behavior.

The second half of this session was devoted to applications of neutron reflectometry, reviewed by

R. K. Thomas (Oxford University), and grazing incidence diffraction, covered by H. Zabel (University of Illinois). Thomas discussed the complementarity of neutron and x-ray reflection techniques for studying inhomogeneities normal to a surface or interface. He gave several examples of reflection measurements on surfactants and polymers adsorbed at the surfaces of solutions which demonstrated the use of contrast variation to enhance the scattering from the adsorbed layer, which is the particular advantage of the neutron technique. In his talk, H. Zabel outlined the basic theory of the novel technique of surface dynamical diffraction and reflection and presented the first neutron results obtained for a Si(110) surface. This technique, which exploits the interplay between simultaneous Bragg diffraction and surface reflection to provide structural information both parallel and normal to a surface, is potentially a powerful probe of surface reconstruction, roughening transitions, and the nature of surface magnetic structures.

The first afternoon session was devoted entirely to reviewing the current status and future plans for the NBS CNRF. NBS Deputy Director Ray Kammer opened the session by outlining the overall scope of the CNRF as a national user facility open to all qualified researchers on the basis of scientific merit. He went on to describe the user policy for the facility and the plan for instrument development which allows for one-third of up to 15 experimental stations to be developed by groups outside NBS, so-called Participating Research Teams, who would then receive three-fourths of the available beam time. Kammer's policy overview was followed by a technical overview by J. M. Rowe of NBS who described the architectural design of the experimental hall and office wing (scheduled for completion in early 1989) associated with the CNRF, and the network of totally reflecting guide tubes that will transport neutrons from the reactor cold source to the CNRF. He also presented data on the performance of the D_2O-ice cold source now in operation in the reactor and gave a timetable for projected instrument development.

The remaining four talks in this session each focused on a specific cold neutron technique and presented design concepts for its implementation in the CNRF. Described were a novel SANS instrument that would utilize a doubly curved mirror to focus a beam onto a detector, the current state of development of neutron supermirrors and their use both to enhance flux and to produce polarized neutron beams, a neutron reflectometer suitable for measurements on both solid and liquid surfaces, and an improved facility for neutron depth profiling which would utilize a converging neutron guide to increase the sensitivity of this technique by more than one order of magnitude over what is now possible using thermal neutrons.

The application of cold neutron methods to the study of submicron structure in specific classes of materials was the theme of the second morning session of the workshop. J. Hayter (Oak Ridge National Laboratory) opened the session with a survey of submicron chemical systems such as colloids and micellar solutions whose structure and interactions can be probed effectively with cold neutrons, while G. Zaccai (Institut Laue-Langevin) gave a corresponding survey of applications to biological systems such as protein solutions and DNA-complexes. Metallurgical applications, with an emphasis on time-resolved studies of phase separation in binary alloys, were reviewed by B. Gaulin (Oak Ridge National Laboratory). Finally, R. Page (Southwest Research Institute) gave a critical review of current and potential applications in the study of damage accumulation, phase transformations, and processing of advanced ceramics.

The final afternoon of the workshop consisted of three discussion sessions which provided participants with the opportunity to comment upon or inquire further about any aspect of the CNRF. The first session on Macromolecular Dynamics explored the potential impact which cold neutron inelastic scattering techniques could have in the study of molecular motions in macromolecular systems. C. Han of the NBS Polymers Division along with Z. Akcasu and S. Krimm, both of the University of Michigan, stimulated the discussion by giving their views of the important scientific issues which could be addressed with advanced neutron scattering instrumentation. This discussion flowed naturally into the next session on Instrumentation and Techniques in which progress in several key areas of cold neutron instrumentation were highlighted. The final session on User Needs focused on the practical needs of the potential user of the CNRF. This discussion was wide-ranging and touched on security requirements for access to the facility, proposal procedures, travel support, housing availability, etc. Several participants stressed the need for adequate sample preparation facilities particularly for biological samples which often have limited lifetimes and thus cannot be prepared far in advance.

One clear impression that emerged from the workshop is that there is a strong and growing in-

terest in the scientific potential of the relatively new techniques of neutron reflectometry and grazing incidence diffraction for the study of near surface and interface structure. As a result of this expressed interest, the development of a state-of-the-art neutron reflectometer for the CNRF will be given increased priority. This instrument, along with a 30 m SANS machine, are expected to be the first instruments to go into operation when the CNRF guide hall is completed.

Copies of the workshop program containing the abstracts of the invited talks, and a 12-page booklet describing the CNRF may be obtained by contacting Carol O'Connor, National Institute of Standards and Technology, Bldg. 235, Rm. A106, Gaithersburg, MD 20899, 301/975-6240.

C. J. Glinka, J. A. Gotaas, and C. O'Connor
Institute for Materials Science and Engineering
National Institute of Standards and Technology
Gaithersburg, MD 20899

Volume 93, Number 6, November–December 1988
Journal of Research of the National Institute of Standards and Technology

Conferences/Events

U.S.-JAPAN PANEL ON WIND AND SEISMIC EFFECTS National Bureau of Standards, Gaithersburg, MD, May 17–20, 1988

The U.S.-Japan Panel on Wind and Seismic Effects provides for cooperative activities of 15 U.S. and 6 Japanese Agencies to reduce damage from strong winds and earthquakes. The Panel is part of the U.S.-Japan Natural Resources Development Program under the aegis of the U.S.-Japan Cooperative Science Program of 1961. The National Bureau of Standards (NBS) provides the U.S.-side chairman and secretariat; Dr. Richard N. Wright, Director of the Center for Building Technology (CBT) and Noel J. Raufaste of CBT, respectively. Annually, the Panel conducts a 1-week joint technical meeting where recent research results are discussed. A technical study tour follows the Panel meetings.

This year (1988) the United States hosted the 20th joint meeting and visits to U.S. laboratories and construction projects. The meeting was held at NBS during 17–20 May. Technical presentations focused on: Wind Engineering; Earthquake Engineering; Storm Surge; Tsunamis; U.S.-Japan Cooperative Research Program (where NBS is performing cooperative research in seismic behavior of large concrete bridge piers); summaries of recent Panel Workshops; and a report from each side on Two Decades of Panel Accomplishments and Future Work.

During 1988–89, the Panel members agreed to performing large-scale testing of precast seismic structural systems, advance technologies in application of active and passive control of buildings and other structures, improve knowledge of strong motion data on performance of buried pipeline systems, and verify the effectiveness of retrofitting and strengthening methods for structures and soils. Five workshops are being planned on: repair and retrofit of buildings, sensor technology applied to large engineered systems, earthquake hazard and risk assessment, disaster prevention for lifeline systems, and loads on bridges. Also, a planning meeting will address remedial treatment of liquefiable soils.

Panel accomplishments during the past year included: more than six guest researchers exchanged between U.S. and Japanese laboratories; correlation of data from the Whittier Narrows and the Mexico City earthquakes with Japanese and U.S. design practices; joint research in large-scale testing of masonry and lifeline structures; sharing repair methods for civil engineering structures; exchanged data from strong motion arrays to study causes and effects of horizontal variations in ground motions and effects of overburden on intensity of ground shaking; and translated into English and published the Japanese publication, *Manual for Repair Methods of Civil Engineering Structures Damaged by Earthquakes.* This report is a valuable reference for development of U.S. building practices. The data produced by the joint Panel influence on-going U.S. and Japan structural engineering research, and guide improvements of building codes and standards of both countries.

Noel J. Raufaste
Center for Building Technology
National Engineering Laboratory
National Institute of Standards and Technology
Gaithersburg, MD 20899

Volume 93, Number 6, November–December 1988
Journal of Research of the National Institute of Standards and Technology

Subject and Author Index to Volume 93

A

Abe, Amy, James E. Freeman, D. Scott Aldrich, and Steven J. Borchert, Pharmaceutical Trace Analysis 242
Abramson, Fred P., and Donald H. Chace, Applications of the Reaction Interface/Mass Spectrometer Technique to the Analysis of Selected Elements and Nuclides from Submicrogram Quantities of Biological Macromolecules and Xenobiotics 419
Absolute Cross-Section Measurements in XQQ Instruments: The NBS Round Robin 431
absorbed dose 603
Accuracy in Analysis: The Role of Standard Reference Materials 213
Accuracy in CPAA for C, N and O and in ERDA and NRA for H 482
Accuracy in Furnace Atomic Absorption Spectroscopy 445
Accuracy in Microanalysis by Electron Energy-Loss Spectroscopy 372
Accuracy in Quantitative Electron Probe Microanalysis 509
Accuracy in the Determination of Chlorinated Dibenzo-p-Dioxins and Dibenzofurans in Environmental Samples 241
Accuracy in Trace Analysis 217
Accuracy of Surface Analyses, The 387
Accurate Measurement of Vitamins in Foods and Tissues 362
accurate trace chemical analysis 228
Ache, H. J., J. M. Torres Llosa, H. Ruf, and K. Schorb, Stripping Voltammetric Assay of Trace Technetium with a TOPO Coated Glassy Carbon Electrode 493
acidic and basic air pollutants 283
Ackerman, Stanley A., John G. Phillips, Donald W. Thayer, Jay B. Fox, Jr., and Ronald K. Jenkins, Effects of Ionizing Radiation on Nutrients in Foods 364
activity coefficients 161
Adams, John R., Michael S. Epstein, Barry I. Diamondstone, and Thomas E. Gills, A New River Sediment Standard Reference Material 234
adipose tissue 343
Adsorptive Stripping Voltammetry—A New Electroanalytical Avenue for Trace Analysis 489
aerosol activation 551
Ahuja, S., G. Thompson, and J. Smith, Trace/Ultratrace Analyses of Unstable Compounds: Investigations on Hydrazobenzene and Azobenzene 344
alcohols 161
Aldrich, D. Scott, Steven J. Borchert, Amy Abe, and James E. Freeman, Pharmaceutical Trace Analysis 242
alkali uranyl(2+)phosphates 557
Alkylation of DNA In Vivo: Development of Analytical Methodology for Trace Quantitative Analysis 419
alkylbenzenes 161
Alofs, D. J., D. E. Hagen, and D. R. White, Condensation Method for Humidity Measurement in the UMR Cloud Simulation Chamber 551
ambient air 281, 279
ambient levels 283
ammonium pyrrolidine dithicarbamate-methyl isobutyl ketone-furnace atomic absorption spectrometry 305
ammonium uranyl(2+)phosphate 557
analysis 213
Analysis at the Atomic Level: The Atom Probe Field-Ion Microscope 374
Analysis of Gaseous and Particle-Associated PAH and Nitroarenes in Ambient Air 279
analysis of PCBs and pesticides in human adipose tissue 343
Analysis of Trace Elements in Methamphetamine Hydrochloride by Inductively Coupled Plasma-Mass Spectrometry 469
analytical balance 565
analytical capabilities of inductively coupled plasma-mass spectrometry 433
analytical chemistry 207
Analytical Chemistry and Material Purity in the Semiconductor Industry 396
analytical electron microscope 369
analytical methodology 419
analyzed reference materials 264
Anderson, T. M., R. E. Thompson, and J. R. Tuschall, U.S. EPA Reference Standards and Quality Assurance Materials for the Analysis of Environmental Pollutants 237
anions to metals 411
Annular Denuders and Filter Packs Designed to Measure Ambient Levels of Acidic and Basic Air Pollutants 283
Application of Flame Spread Theory to Predict Material Performance, The 61
application of reduced palladium as a chemical modifier 450
Applications of Lasers in Bioanalytical Chemistry 502
Applications of Mass Spectrometry in Polymer Analysis: Use of GC-GC-High Resolution MS to Identify Photo- and Oxidative Degradation Products of BPA-Polycarbonate 394

Applications of the Reaction Interface/Mass Spectrometer Technique to the Analysis of Selected Elements and Nuclides from Submicrogram Quantities of Biological Macromolecules and Xenobiotics 419
Appropriate Reference Parameters for the Evaluation of Elemental Analysis Data from Biomedical Specimens 326
arc (argon, blackbody, and hydrogen) 21
Arey, Janet, Barbara Zielinska, Roger Atkinson, and Arthur M. Winer, Analysis of Gaseous and Particle-Associated PAH and Nitroarenes in Ambient Air 279
argon 85
aromatic compounds in natural samples by Shpol'skii Spectroscopy 441
arsenic species in urine 315
Arunachalam, J., S. Jaikumar, S. V. Burangey, S. Gangadharan, and S. Natarajan, Multitechnique Approach to Trace Characterization of High Purity Materials: Gallium 400
Assessment of the Analytical Capabilities of Inductively Coupled Plasma-Mass Spectrometry 433
Atkinson, Roger, Arthur M. Winer, Janet Arey, and Barbara Zielinska, Analysis of Gaseous and Particle-Associated PAH and Nitroarenes in Ambient Air 279
atom probe field-ion microscope 374
atomic absorption spectrometric applications to clinical-biomedical trace metal analyses 334
atomic absorption spectrometry 350
atomic level 374
atomic spectroscopy 447
automated interpretation of large EPMA data sets 260
Automated Manufacturing Research Facility 539
Automation and Application of a Direct-Current Plasma Emission Spectrometer 458
azobenzene 344

B

Bailey, George G., and Daniel C. Paschal, Determination of Manganese in Serum with Zeeman Effect Graphite Furnace Atomic Absorption 323
Barker, Todd Q., Harlan R. Wilk, Steven L. Monfre, and Steven D. Brown, Multicomponent Analysis in Static and Flow Systems Using Digital Filters 253
Barnan, B. N., Daniel E. Martire, and Michele (Miller) Schantz, Partitioning of Alkylbenzenes and Aliphatic Alcohols between Hexadecane and Methanol-Water Mixtures 161
Bavdaz, M., N. Gurker, P. Ketelsen, W. Petersen, M.H. Salehi, T. Dietrich, and A. Knöchel, Synchrotron Radiation Excited Fluorescence Micro-Analysis Using a New Imaging Technique 379
Beach, L. M., T. M. Rettberg, and D. E. Shrader, Graphite Furnace AAS: Application of Reduced Palladium as a Chemical Modifier 450
Beekman, D. W., E. H. Taylor, V. Lorch, L. J. Moore, J.E. Parks, and M. T. Spaar, Ultra-Trace Elemental and Isotopic Quantification for Neonatal Nutrition Studies 328
Behne, Dietrich, and Venkatesh Iyengar, Appropriate Reference Parameters for the Evaluation of Elemental Analysis Data From Biomedical Specimens 326
Bellama, Jon M., Richard A. Durst, and Rosanne Kannuck, Homogeneous Electrochemical Immunoassay Using a Chemically Modified Electrode 506
Berman, Eleanor, Some Atomic Absorption Spectrometric Applications to Clinical-Biomedical Trace Metal Analyses 334
Beugelsdijk, Tony J., and Dan W. Knobeloch, Laboratory Robotics in Radiation Environments 268
Biochemical Applications of Chromatography/SIMS 499
biological macromolecules 419
biological reference materials 360
Biological Reference Materials for Trace Element Analysis: What is New? 318
blackbody 7
Blyshak, L., S. L. Neal, I. M. Warner, G. Nelson, and G. Patonay, Enhanced Multidimensional Luminescence Measurements Through Cyclodextrin Complexation 438
BOD_5 311
Borchert, Steven J., Amy Abe, James E. Freeman, and D. Scott Aldrich, Pharmaceutical Trace Analysis 242
BPA-Polycarbonate 394
Braun, Walter, Philippe Dagaut, and Barry C. Cadoff, Kinetic Studies Using a Highly Sensitive Microphone Detector 643
Bridges, J. Mervin, William R. Ott, and Jules Z. Klose, Radiometric Calibrations of Portable Sources in the Vacuum Ultraviolet 21
Brown, D., G. Legere, and P. Burgener, ICP Trace Element Analyses from Fusion Dissolution 454
Brown, R., N. E. Sanderson, P. Charalambous, and D. J. Hall, Quantitative Aspects of Glow Discharge Mass Spectrometry 426
Brown, K. K., P. Tomboulian, and S.M. Walters, Trace Level Quantitation of Phenyltin Compounds Using HPTLC 301
Brown, Steven D., Todd Q. Barker, Harlan R. Wilk, and Steven L. Monfre, Multicomponent Analysis in Static and Flow Systems Using Digital Filters 253
Brown, W. E., M. S. Tung, N. Eidelman, and B. Sieck, Octacalcium Phosphate Solubility Product from 4 to 37 °C 613
Bruno, Thomas J., Solvent-Free Injection in Supercritical Fluid Chromatography Using Sintered Glass Deposition 655
Buckley, T. J., and J.M. Rukkers, A Computer Controlled Data Acquisition System for Combustion Calorimetric Experiments, ... 145

Bulkin, Bernard J., The Importance of Quantitative Trace Analysis in Industry Today 189
Burangey, S. V., S. Gangadharan, S. Natarajan, J. Arunachalam, and S. Jaikumar, Multitechnique Approach to Trace Characterization of High Purity Materials: Gallium 400
Burgener, P., D. Brown., and G. Legere, ICP Trace Element Analyses from Fusion Dissolution 454
Busch, K. L., M.S. Stanley, K. L. Duffin, and J. C. Dunphy, Biochemical Applications of Chromatography/SIMS 499
Byrd, G. D., L. T. Sniegoski, and E. White V, Determination of 3-Quinuclidinyl Bezilate in Urine 293

C

Cadoff, Barry C., Walter Braun, and Philippe Dagaut, Kinetic Studies Using a Highly Sensitivie Microphone Detector 643
calibration 7, 53, 565
calibration, grid plate 41
calibration, radiometric 21
calibration standards 264
calibration, uncertainty 53
calibrations of portable sources in the vacuum ultraviolet 21
calorimeter 603
capillary electrophoresis 406
CAPPIS 298
carbon-11 labelled carboxylic acids 338
Carroll, Raymond J., Clifford H. Spiegelman, and Robert L. Watters, Jr., Heteroscedastic Calibration Using Analyzed Reference Materials as Calibration Standards 264
Caruso, Joseph A., Microwave Induced Plasmas as Sources for Atomic Spectroscopy 447
Chabala, J., Y. L. Wang, and R. Levi-Setti, Imaging Microanalysis of Materials With a Finely Focused Heavy Ion Probe 377
Chace, Donald H., and Fred P. Abramson, Applications of the Reaction Interface/Mass Spectrometer Technique to the Analysis of Selected Elements and Nuclides from Submicrogram Quantities of Biological Macromolecules and Xenobiotics 419
Chaconas, Karen, J., and Marilyn Nashman, The NBS Vision System in the AMRF 539
Chang, C.-j., R. G. Cooks, and J. R. O'Lear, Alkylation of DNA In Vivo: Development of Analytical Methodology for Trace Quantitative Analysis 419
Chang, S. C., T. S. Kao, C. P. Tang, and M.R. Lee, Studies of Limit of Detection on 2,4,6-Trinitrotoluene (TNT) by Mass Spectrometry 428
Characterization of High Purity Silicides 239
Charalambous, P., D. J. Hall, R. Brown, and N.E. Sanderson, Quantitative Aspects of Glow Discharge Mass Spectrometry 426
chemical blanks and chemical yields 228
chemically active electrode materials 488
chemically modified electrode 506
Chemiluminescence Detection in Flowing Streams—Immobilized and Solid-State Reagents 501
Chemometrics in Europe: Selected Results 257
Chemometrics and Standards 193
Cheung, Y. Y., C. W. McLeod, Y. Zhang, I. Cook, A. Cox, and A. R. Date, Flow Injection-Inductively Coupled Plasma Spectrometry: A New Strategy for Ultratrace Analysis 462
chlorinated dibenzo-p-dioxins 241
chromatography 655
chromatography, biochemical applications 499
chromatography, ion 411, 425
chromatography, open tubular liquid 403
chromatography, supercritcal fluid 409, 655
Chromium (III) and Chromium (VI) 305
Ciaccio, Leonard L., and Klaus Hameyer, An Instrument for Determination of Energy Oxygen and BOD_5 311
Classical Pitfalls in Contemporary Nuclear Data Analysis 479
clinical chemical analysis 336
cloud drop growth 551
CO_2 laser 643
Cohen, A., P. Ellerbe, R. Schaffer, L. T. Sniegoski, E. White V, and M. J. Welch, The Development of Definitive Methods for Organic Serum Constituents 341
combustion 145
compositional mapping 518
Computer Assisted Pesticide and PCB Identification System (CAPPIS) 298
computer application 145
Computer Controlled Data Acquisition System for Combustion Calorimetric Experiments, A 145
computer vision 539
Condensation Method for Humidity Measurement in the UMR Cloud Simulation Chamber 551
Conlon, T. W., and J. A. Cookson, MeV Ion Beam Analysis 473
contamination or trends in the concentrations of trace metals in marine environments 321
convection 603
convective velocity 603
Convective Velocity Effects on a Thermistor in Water 603
Cook, Edgar, Mirtha Umãna, Jess Waller, Mansukh Wani, and Carol Whisnant, Enzyme-Enhanced Electrochemical Immunoassay for Phenytoin 659
Cook, I., A. Cox, A. R. Date, Y. Y. Cheung, C. W. McLeod, and Y. Zhang, Flow Injection-Inductively Coupled Plasma Spectrometry: A New Strategy for Ultratrace Analysis 462
Cooks, R. G., J. R. O'Lear, and C.-j. Chang, Alkylation of DNA In Vivo: Development of Analytical Methodology for Trace Quantitative Analysis 419

Cookson, J. A., and T. W. Conlon, MeV Ion Beam Analysis..... 473
Cox, A., A. R. Date, Y. Y. Cheung, C. W. McLeod, Y. Zhang, and I. Cook, Flow Injection-Inductively Coupled Plasma Spectrometry: A New Strategy for Ultratrace Analysis..... 462
CPAA..... 482
Crecelius, Eric A., Detecting Contamination or Trends in the Concentrations of Trace Metals in Marine Environments..... 321
Crews, H. M., R. Massey, D. J. McWeeny, and J. R. Dean, Trace Element Speciation in Food: A Combined Enzymolysis–SEC-ICP-MS Approach..... 349
Crews, H. M., R. C. Massey, D. J. McWeeny, J.R. Dean, and L. Ebdon, Some Applications of Isotope Analysis of Lead in Food by ICP-MS..... 464
Crilly, Paul Benjamin, An Evaluation of Jansson's Method to Deconvolve Overlapped Gas Chromatographic Peaks..... 413
cryogenic size reduction..... 292
crystal growth..... 577
Currie, Lloyd A., George A. Klouda, and Ann E. Sheffield, Trace Radiocarbon Analysis of Environmental Samples..... 289
Currie, L. A., Chemometrics and Standards..... 193
cyclodextrin complexation..... 438
Czae, Myung-Zoon, and Jong-Hyup Lee, Range-Programming Stripping Voltammetry for Determination of Some Metals in Seawater..... 296

D

Dagaut, Philippe, Barry C. Cadoff, and Walter Braun, Kinetic Studies Using a Highly Sensitive Microphone Detector..... 643
data acquisition..... 145
Date, A. R., Y. Y. Cheung, C. W. McLeod, Y. Zhang, I. Cook, and A. Cox, Flow Injection-Inductively Coupled Plasma Spectrometry: A New Strategy for Ultratrace Analysis..... 462
Davis, R. S., and B. E. Welch, Practical Uncertainty Limits to the Mass Determination of a Piston-Gage Weight..... 565
Davis, R. S., M. R. Moldover, J. P. M. Trusler, T. J. Edwards, and J. B. Mehl, Measurement of the Universal Gas Constant *R* Using a Spherical Acoustic Resonator..... 85
De Bièvre, Paul, Transferring Accuracy to the Trace Level and Then to the Field..... 520
De Wit, J. S. M., J. W. Jorgenson, R. T. Kennedy, R. L. St. Claire, III, J. G. White, and P. R. Dluzneski, Open Tubular Liquid Chromatography and the Analysis of Single Neurons..... 403
De Kesel, A., J. Hoste, B. Wallaeys, J. Vandenhaute, J. Versieck, and L. Vanballenberghe, Biological Reference Materials for Trace Element Analysis: What is New?..... 318
Dean, J. R., H. M. Crews, R. Massey, and D. J. McWeeny, Trace Element Speciation in Food: A Combined Enzymolysis–SEC-ICP-MS Approach..... 349
Dean, J. R., L. Ebdon, H. M. Crews, R. C. Massey, and D. J. McWeeny, Some Applications of Isotope Analysis of Lead in Food by ICP-MS..... 464
Dennis, M. J., N. Howarth, R. C. Massey, D. J. McWeeny, I. Parker, M. Scotter, and J. R. Startin, Ethyl Carbamate Analysis in Fermented Products: A Comparsion of Measurements of Mass Spectrometry, Thermal Energy Analyser, and Hall Electrolytic Conductivity Detector..... 249
Depth Profiling of Trace Constituents Using Secondary Ion Mass Spectrometry..... 390
Design of Cost-Effective QC Procedures for Clinical Chemistry..... 218
Detecting Contamination or Trends in the Concentrations of Trace Metals in Marine Environments..... 321
Determination of Chromium (III) and Chromium (VI) by Ammonium Pyrrolidine Dithiocarbamate-Methyl Isobutyl Ketone-Furnace Atomic Absorption Spectrometry..... 305
Determination of Manganese in Serum with Zeeman Effect Graphite Furnace Atomic Absorption..... 323
Determination of 3-Quinuclidinyl Benzilate in Urine..... 293
Determination of Trace Elements in Uranium Oxide (U_3O_8) by Inductively Coupled Plasma Emission Spectrometry and Graphite Furnace Atomic Absorption Spectrometry, The..... 452
Determination of Tributyltin in the Marine Environment..... 277
Determination of Traces of Uranium and Thorium in Microelectronics Constituent Materials..... 398
determination of vitamin C in milk..... 367
development of analytical methodology for trace quantitative analysis..... 419
Development of Definitive Methods for Organic Serum Constituents, The..... 341
Development of Multi-Purpose Biological Reference Materials..... 360
de Wit, J. S. M., J. W. Jorgenson, R. T. Kennedy, R. L. St. Claire III, J. G. White, and P. R. Dluzneski, Open Tubular Liquid Chromatography and the Analysis of Single Neurons..... 403
DeZwaan, Jack, and Douglas B. Hooker, Organic Microanalysis of Submicrogram Samples..... 245
diagnostic probe..... 484
Diamondstone, Barry I., Thomas E. Gills, John R. Adams, and Michael S. Epstein, A New River Sediment Standard Reference Material,..... 234

dibenzo-p-dioxins 241
dibenzofurans 241
Dierkes, Joseph E., Computer Assisted Pesticide and PCB Identification System (CAPPIS)..... 298
Dietrich, T., A. Knöchel, M. Bavdaz, N. Gurker, P. Ketelsen, W. Petersen, and M. H. Salehi, Synchrotron Radiation Excited Fluorescence Micro-Analysis Using a New Imaging Technique 379
Diffraction Imaging (Topography) with Monochromatic Synchrotron Radiation..... 577
digital filters 253
direct-current plasma emission spectrometer 458
direct digital synthesis..... 53
Direct Solids Analysis Using Sputter Initiated Resonance Ionization Spectroscopy (SIRIS) 383
dithiocarbamates and related compounds..... 496
Djordjevic, Nebojsa, Karin E. Markides, and Milton L. Lee, Supercritical Fluid Chromatography: Application to Trace Analysis..... 409
Dluzneski, P. R., J. S. M. de Wit, J. W. Jorgenson, R. T. Kennedy, R. L. St. Claire III, and J. G. White, Open Tubular Liquid Chromatography and the Analysis of Single Neurons 403
DNA 419
Dobbyn, Ronald C., Uri Laor, Bruce Steiner, and Masao Kuriyama, Diffraction Imaging (Topography) with Monochromatic Synchrotron Radiation..... 577
Doiron, Theodore D., Grid Plate Calibration at the National Bureau of Standards..... 41
Domen, Steve R., Convective Velocity Effects on a Thermistor in Water 603
Doyle, Matthew J., D. Scott Wright, H. Brian Halsall, William R. Heineman, Sarah H. Jenkins, and Kenneth R. Wehmeyer, Electrochemical Enzyme Immunoassay..... 491
Duffin, K. L., J. C. Dunphy, K. L. Busch and M. S. Stanley, Biochemical Applications of Chromatography/SIMS 499
Dunn, William J., III, S. L. Emery, and Donald R. Scott, Pattern Recognition Classification and Identification of Trace Organic Polutants in Ambient Air from Mass Spectra..... 281
Dunphy, J. C., K. L. Busch, M. S. Stanley, and K. L. Duffin, Biochemical Applications of Chromatography/SIMS 499
Durst, R., S. Gomiscek, M. Verber, and V. Francetic, Electrochemical Studies of Dithiocarbamates and Related Compounds..... 496
Durst, Richard A., Laurie Locascio-Brown, and Anne L. Plant, Liposome-Based Flow Injection Immunoassay System 663
Durst, Richard A., Rosanne Kannuck, and Jon M. Bellama, Homogeneous Electrochemcial Immunoassy Using a Chemically Modified Electrode..... 506

E

Eatherton, Randy L., and Herbert H. Hill, Jr., Ion Mobility Spectrometry after Chromatography—Accomplishments, Goals, Challenges..... 425
Ebdon, L., H. M. Crews, R. C. Massey, D. J. McWeeny, and J.R. Dean, Some Applications of Isotope Analysis of Lead in Food by ICP-MS 464
Edwards, T. J., J.B. Mehl, R. S. Davis, M. R. Moldover, and J. P. M. Trusler, Measurement of the Universal Gas Constant *R* Using a Spherical Acoustic Resonator 85
Effects of Ionizing Radiation on Nutrients in Foods..... 364
Egerton, Ray F., Accuracy in Microanalysis by Electron Energy-Loss Spectroscopy..... 372
Eidelman, N., B. Sieck, W. E. Brown, and M. S. Tung, Octacalcium Phosphate Solubility Product from 4 to 37 °C..... 613
Elder, Robert S., Statistical Models in Quality Control for Trace Analysis 221
electroanalytical avenue for trace analysis..... 489
Electrochemical Enzyme Immunoassay 491
Electrochemical Studies of Dithiocarbamates and Related Compounds..... 496
electron energy-loss spectroscopy..... 372
electron probe microanalysis 509
electrooptic materials..... 577
elemental analysis..... 269
Ellerbe, P., L. T. Sniegoski, J. M. Miller, and E. White V, An Isotope Dilution Mass Spectrometric (IDMS) Method for the Determination of Vitamin C in Milk, ... 367
Ellerbe, P., R. Schaffer, L. T. Sniegoski, E. White V, M. J. Welch, and A. Cohen, The Development of Definitive Methods for Organic Serum Constituents..... 341
Emery, S. L., Donald R. Scott, and William J. Dunn III, Pattern Recognition Classification and Identification of Trace Organic Polutants in Ambient Air from Mass Spectra..... 281
energy oxygen..... 311
energy transfer 643
Enhanced Multidimensional Luminescence Measurements Through Cyclodextrin Complexation 438
environmental samples..... 289, 307
Enzyme-Enhanced Electrochemical Immunoassay for Phenytoin..... 659
enzymolysis, combined 349
epithermal neutron activation..... 224
Epler, K. S., T. C. O'Haver, M. S. Epstein, and R. E. Jenkins, Automation and Application of a Direct-Current Plasma Emission Spectrometer..... 458
EPMA data sets 260
Epstein, Michael S., Barry I. Diamondstone, Thomas E. Gills, and John R. Adams, A New River Sediment Standard Reference Material 234

Epstein, M. S., R. E. Jenkins, K. S. Epler, and T. C. O'Haver, Automation and Application of a Direct-Current Plasma Emission Spectrometer 458
equilibrium constants 613
error estimation in gamma-ray spectrometry 481
Espourteille, F. A., C. D. Rice, R. G. Huggett, and M. A. Unger, Determination of Tributyltin in the Marine Environment 277
Ethyl Carbamate Analysis in Fermented Products: A Comparsion of Measurements of Mass Spectrometry, Thermal Energy Analyser, and Hall Electrolytic Conductivity Detector 249
evaluation of elemental analysis data from biomedical specimens 326
Evaluation of Jansson's Method to Deconvolve Overlapped Gas Chromatographic Peaks, An 413
Evenson, Merle A., Inaccuracies in Clinical Chemical Analysis 336
Evolutionary Factor Analysis 256
Ewald, M., P. Garriques, and E. Parlanti, Trace Analysis of Aromatic Compounds in Natural Samples by Shpol'skii Spectroscopy 441
expansion cloud chamber 551
expert system 260
Expert Systems and Robotics 209
exposure assessment studies 315
extraction 274

F

factor analysis 256
Factor, Arnold, Ralph J. May, and Woodfin V. Ligon, Jr., Applications of Mass Spectrometry in Polymer Analysis: Use of GC-GC-High Resolution MS to Identify Photo- and Oxidative Degradation Products of BPA-Polycarbonate 394
Fairbank, W. M., Jr., J. M. R. Hutchinson, J. E. Parks, M. T. Spaar, and L. J. Moore, Direct Solids Analysis Using Sputter Initiated Resonance Ionization Spectroscopy (SIRIS) 383
Fassett, J. D., Inorganic Trace Analysis by Isotope Dilution Mass Spectrometry—New Frontiers 417
Fast-Neutron Diagnostic Probe, A 484
fermented products 249
Field, Bruce, and Liu Ruimin, An Improvement in the Reliability of Standard Cell Enclosures 533
filter packs 283
Finn, Ronald, and Patricia Landais, Technical Difficulties Associated With the Formation of Carbon-11 Labelled Carboxylic Acids 338
flame spread 61
flow calorimetry 145
Flow Injection-Inductively Coupled Plasma Spectrometry: A New Strategy for Ultratrace Analysis 462
Fluorescence Spectrometric Determination of Nonfluorescent Compounds via Molecular Fragmentation 437
fluorescent and chemiluminescent detection in HPLC 504
fluorometrix analysis 443
food analysis 358
formation of carbon-11 labelled carboxylic acids 338
Fox, Jay B., Jr., Ronald K. Jenkins, Stanley A. Ackerman, John G. Phillips, and Donald W. Thayer, Effects of Ionizing Radiation on Nutrients in Foods 364
Francetic, V., R. Durst, S. Gomiscek, and M. Veber, Electrochemical Studies of Dithiocarbamates and Related Compounds 496
Freeman, James E., D. Scott Aldrich, Steven J. Borchert, and Amy Abe, Pharmaceutical Trace Analysis 242
Frost, J. H., J. H. Phillips, C. A. Potera, and P. M. Michalko, The Use of Cryogenic Size Reduction to Improve Purgeable Priority Pollutant Analyses in Soil Samples 292
fundamental constants 85
furnace atomic absorption spectroscopy 445
fusion dissolution 454

G

gallium 400
gamma-ray spectrometry 481
Gangadharan, S., S. Natarajan, J. Arunachalam, S. Jaikumar, and S. V. Burangey, Multitechnique Approach to Trace Characterization of High Purity Materials: Gallium 400
Garbarino, J. R., and H. E. Taylor, Assessment of the Analytical Capabilities of Inductively Coupled Plasma-Mass Spectrometry 433
Garrigues, P., E. Parlanti, and M. Ewald, Trace Analysis of Aromatic Compounds in Natural Samples by Shpol'skii Spectroscopy 441
gas phase 643
GC/MS 331, 365
geological samples 224
geometry correction 41
Gilbert, John, and James R. Startin, Stable Isotope Dilution GC/MS for the Quantification of Food Contaminants 365
Gills, Thomas E., John R. Adams, Michael S. Epstein, and Barry I. Diamondstone, A New River Sediment Standard Reference Material 234
glow discharge mass spectrometry 392, 426
Gomiscek, S., M. Veber, V. Francetic, and R. Durst, Electrochemical Studies of Dithiocarbamates and Related Compounds 496

Gordon, C. M., C. W. Peters, and T. K. Olson, A Fast-Neutron Diagnostic Probe 484
Graphite Furnace AAS: Application of Reduced Palladium as a Chemical Modifier 450
graphite furnace analysis 307
graphite furnace atomic absorption spectrometry 323, 452, 467
Grasserbauer, M., Quantitative Secondary Ion Mass Spectrometry 510
grid plate 41
Grid Plate Calibration at the National Bureau of Standards 41
Gurker, N., P. Ketelsen, W. Petersen, M. H. Salehi, T. Dietrich, A. Knöchel, and M. Bavdaz, Synchrotron Radiation Excited Fluorescence Micro-Analysis Using a New Imaging Technique 379

H

Haag, Werner R., Measurement of Sunlight-Induced Transient Species in Surface Waters 285
Hagen, D. E., D. R. White, and D. J. Alofs, Condensation Method for Humidity Measurement in the UMR Cloud Simulation Chamber 551
Hall, D. J., R. Brown, N. E. Sanderson, and P. Charalambous, Quantitative Aspects of Glow Discharge Mass Spectrometry 426
Hall electrolytic conductivity detector 249
Halsall, H. Brian, William R. Heineman, Sarah H. Jenkins, Kenneth R. Wehmeyer, Matthew J. Doyle, and D. Scott Wright, Electrochemical Enzyme Immunoassay 491
Hameyer, Klaus, and Ciaccio, Leonard L., An Instrument for Determination of Energy Oxygen and BOD_5 311
heat transfer 61
heavy ion probe 377
Heineman, William R., Sarah H. Jenkins, Kenneth R. Wehmeyer, Matthew J. Doyle, D. Scott Wright, and H. Brian Halsall, Electrochemical Enzyme Immunoassay 491
Heinrich, K. F. J., Accuracy in Quantitative Electron Probe Microanalysis 509
Herold, David A., Judy C. Hundley, Michael R. Wills, John Savory, and Michael Kinter, Use of High Resolution GC/MS for Obtaining Accuracy in Lipid Measurements 331
Heteroscedastic Calibration Using Analyzed Reference Materials as Calibration Standards 264
hexadecane 161
Heydorn, K., Classical Pitfalls in Contemporary Nuclear Data Analysis 479
hierarchical design 539
High Performance Capillary Electrophoresis 406
high purity materials 400
high purity silicides 239
high resolution GC/MS 331
High Resolution Nonlinear Laser Spectroscopy 440
Hill, Herbert H., Jr., and Randy L. Eatherton, Ion Mobility Spectrometry after Chromatography—Accomplishments, Goals, Challenges 425
History of Trace Analysis 175
Holler, J. S., D. G. Patterson, and S. J. Smith, Quantification of Toxic Chemicals in Selected Human Populations 412
Homogeneous Electrochemical Immunoassay Using a Chemically Modified Electrode 506
Hooker, Douglas B., and Jack DeZwaan, Organic Microanalysis of Submicrogram Samples 245
Hoste, J., B. Wallaeys, J. Vandenhaute, J. Versieck, L. Vanballenberghe, and A. De Kesel, Biological Reference Materials for Trace Element Analysis: What is New? 318
Hotes, S. A., and W. R. Kelly, Importance of Chemical Blanks and Chemical Yields in Accurate Trace Chemical Analysis 228
Howarth, N., R. C. Massey, D. J. McWeeny, I. Parker, M. Scotter, J. R. Startin, and M. J. Dennis, Ethyl Carbamate Analysis in Fermented Products: A Comparsion of Measurements of Mass Spectrometry, Thermal Energy Analyser, and Hall Electrolytic Conductivity Detector 249
HPLC 504
HPTLC 301
Huber, Calvin O., Voltammetric Sensors Using Chemically Active Electrode Materials 488
Huggett, R. G., M. A. Unger, F. A. Espourteille, and C. D. Rice, Determination of Tributyltin in the Marine Environment 277
humidity measurement 551
Hundley, Judy C., Michael R. Wills, John Savory, Michael Kinter, and David A. Herold, Use of High Resolution GC/MS for Obtaining Accuracy in Lipid Measurements 331
Huneke, J. C., Relative Sensitivity and Quantitation in Glow Discharge Mass Spectrometry: A Progress Report 392
Hutchinson, J. M. R., J. E. Parks, M. T. Spaar, L. J. Moore, and W. M. Fairbank, Jr., Direct Solids Analysis Using Sputter Initiated Resonance Ionization Spectroscopy (SIRIS) 383
hydrazobenzene 344
hydrolysis 613

I

Ianniello, Robert M., Trace Analyses of Impurities in Povidone by Square Wave Voltammetry 487
ICP Trace Element Analyses from Fusion Dissolution 454
ICP-AES: A Realistic Assessment of Its Capabilities for Food Analysis 358
ICP-MS 464
ideal gas 85
IDMS 367

ignition 61
Ihnat, Milan, Reliable Measurement of Major, Minor, and Trace Elemental Nutrients 354
Imaging Microanalysis of Materials With a Finely Focused Heavy Ion Probe 377
image processing 539
imaging technique 379
Importance of Chemical Blanks and Chemical Yields in Accurate Trace Chemical Analysis 228
Importance of Quality Assurance in Trace Analysis, The 232
Importance of Quantitative Trace Analysis in Industry Today, The 189
Improvement in the Reliablity of Standard Cell Enclosures, An 533
Improving Accuracy in Graphite Furnace Atomic Absorption Spectrometry Through Peak Shape Monitoring 467
impurities in povidone by square wave voltammetry 487
Inaccuracies in Clinical Chemical Analysis 336
Increased Accuracy in the Automated Interpretation of Large EPMA Data Sets by the Use of an Expert System 260
In-Situ Filtration Sampler for the Measurement of Trace Metals in Precipitation 312
inductively coupled plasma-mass spectrometry 469
injection 655
Inorganic Trace Analysis by Isotope Dilution Mass Spectrometry—New Frontiers 417
Instrument for Determination of Energy Oxygen and BOD_5, An 311
international comparison 545
International Comparisons of Pressure Standards: A Status Report 545
ion beam analysis 473
Ion Chromatography: From Anions to Metals 411
Ion Mobility Spectrometry after Chromatography—Accomplishments, Goals, Challenges 425
ionizing radiation on nutrients in foods 364
irradiance 21
Isenhour, T. L. and J. C. Marshall, Expert Systems and Robotics 209
isotope analysis of lead in food 464
Isotope Dilution Mass Spectrometry (IDSM) 419
Isotope Dilution Mass Spectrometric (IDMS) Method for the Determination of Vitamin C in Milk, An 367
isotopic quantification 328
Iyengar, Venkatesh, and Dietrich Behne, Appropriate Reference Parameters for the Evaluation of Elemental Analysis Data From Biomedical Specimens 326
Iyengar, Venkatesh, James Tanner, Wayne Wolf, and Rolf Zeisler, Development of Multi-Purpose Biological Reference Materials 360

J

Jackson, John K., Donald A. McSparron, James H. Walker, and Robert D. Saunders, The NBS Scale of Spectral Irradiance 7
Jaikumar, S., S. V. Burangey, S. Gangadharan, S. Natarajan, and J. Arunachalam, Multitechnique Approach to Trace Characterization of High Purity Materials: Gallium 400
Janssens, K., W. Van Borm, and P. Van Espen, Increased Accuracy in the Automated Interpretation of Large EPMA Data Sets by the Use of an Expert System 260
Jansson's Method 413
Jassie, L. B., and H. M. Kingston, Microwave Acid Sample Decomposition for Elemental Analysis 269
Jenkins, Sarah H., Kenneth R. Wehmeyer, Matthew J. Doyle, D. Scott Wright, H. Brian Halsall, and William R. Heineman, Electrochemical Enzyme Immunoassay 491
Jenkins, R. E., K. S. Epler, T. C. O'Haver, and M. S. Epstein, Automation and Application of a Direct-Current Plasma Emission Spectrometer 458
Jenkins, Ronald K., Stanley A. Ackerman, John G. Phillips, Donald W. Thayer, and Jay B. Fox, Jr., Effects of Ionizing Radiation on Nutrients in Foods 364
Jones, J. W., ICP-AES: A Realistic Assessment of Its Capabilities for Food Analysis 358
Jorgenson, J. W., R. T. Kennedy, R. L. St. Claire III, J. G. White, P. R. Dluzneski, and J. S. M. de Wit, Open Tubular Liquid Chromatography and the Analysis of Single Neurons 403
Junk, Gregor A., and John J. Richard, Solid Phase Extraction on a Small Scale 274

K

Kalman, David A., Quantitation of Arsenic Species in Urine for Exposure Assessment Studies 315
Kannuck, Rosanne, Jon M. Bellama, and Richard A. Durst, Homogeneous Electrochemical Immunoassy Using a Chemically Modified Electrode 506
Kao, T. S., C. P. Tang, M. R. Lee, and S. C. Chang, Studies of Limit of Detection on 2,4,6-Trinitrotoluene (TNT) by Mass Spectrometry 428
Karger, B. L., High Performance Capillary Electrophoresis 406
Kateman, G., Accuracy in Trace Analysis 217
Kawasaki, T., O. Wong, C. Wang, and T. Kuwana, Trace Biogenic Amine Analysis with Pre-Column Derivatization and with Fluorescent and Chemiluminescent Detection in HPLC 504
Keller, Barbara J., In-Situ Filtration Sampler for the Measurement of Trace Metals in Precipitation 312

Kelly, W. R., and S. A. Hotes, Importance of Chemical Blanks and Chemical Yields in Accurate Trace Chemical Analysis..... 228
Kennedy, R. T., R. L. St. Claire III, J. G. White, P. R. Dluzneski, J. S. M. de Wit, and J. W. Jorgenson, Open Tubular Liquid Chromatography and the Analysis of Single Neurons..... 403
Ketelsen, P., W. Petersen, M. H. Salehi, T. Dietrich, A Knöchel, M. Bavdaz, and N. Gurker, Synchtroton Radiation Excited Fluorescence Micro-Analysis Using a New Imaging Technique..... 379
Kinetic Studies Using a Highly Sensitive Microphone Detector..... 643
kinetics..... 643
Kingston, H. M., and L. B. Jassie, Microwave Acid Sample Decomposition for Elemental Analysis..... 269
Kinter, Michael, David A. Herold, Judy C. Hundley, Michael R. Wills, and John Savory, Use of High Resolution GC/MS for Obtaining Accuracy in Lipid Measurements..... 331
Kishi, Tohru, Analysis of Trace Elements in Methamphetamine Hydrochloride by Inductively Coupled Plasma-Mass Spectrometry..... 469
Klose, Jules Z., J. Mervin Bridges, and William R. Ott, Radiometric Calibrations of Portable Sources in the Vacuum Ultraviolet..... 21
Klouda, George A., Ann E. Sheffield, and Lloyd A. Currie, Trace Radiocarbon Analysis of Enviornmental Samples..... 289
Knobeloch, Dan, and Tony J. Beugelskijk, Laboratory Robotics in Radiation Environments..... 268
Knöchel, A., M. Bavdaz, N. Gurker, P. Ketelsen, W. Petersen, M. H. Salehi, and T. Dietrich, Synchrotron Radiation Excited Fluorescence Micro-Analysis Using a New Imaging Technique..... 379
Koch, William F., Ion Chromatography: From Anions to Metals..... 411
Kowalski, Bruce R., Process Analytical Chemistry..... 207
Kuriyama, Masao, Ronald C. Dobbyn, Uri Laor, and Bruce Steiner, Diffraction Imaging (Topography) with Monochromatic Synchrotron Radiation..... 577
Kuwana, T., T. Kawasaki, O. Wong, and C. Wang, Trace Biogenic Amine Analysis with Pre-Column Derivatization and with Fluorescent and Chemiluminescent Detection in HPLC..... 504

L

Laboratory Robotics in Radiation Environments..... 268
Laitinen, H. A., History of Trace Analysis..... 175
lamp (deuterium)..... 21
Lampaarski, L. L. and T. J. Nestrick, Accuracy in the Determination of Chlorinated Dibenzo-p-Dioxins and Dibenzofurans in Environmental Samples..... 239
Landais, Patricia, and Ronald Finn, Technical Difficulties Associated With the Formation of Carbon-11 Labelled Carboxylic Acids..... 338
Laor, Uri, Bruce Steiner, Masao Kuriyama, and Ronald C. Dobbyn, Diffraction Imaging (Topography) with Monochromatic Synchrotron Radiation..... 577
lasers in bioanalytical chemistry..... 502
Lee, Jong-Hyup and Myung-Zoon Czae, Range-Programming Stripping Voltammetry for Determination of Some Metals in Seawater..... 296
Lee, M. R., S. C. Chang, T. S. Kao, and C. P. Tang, Studies of Limit of Detection on 2,4,6-Trinitrotoluene (TNT) by Mass Spectrometry..... 428
Lee, Milton L., Nebojsa Djordjevic, and Karin E. Markides, Supercritical Fluid Chromatography: Application to Trace Analysis..... 409
Legere, G., P. Burgener, and D. Brown, ICP Trace Element Analyses from Fusion Dissolution..... 454
Levi-Setti, R., J Chabala, and Y. L. Wang, Imaging Microanalysis of Materials with a Finely Focused Heavy Ion Probe..... 377
Ligon, Woodfin, V., Jr., Arnold Factor, and Ralph J. May, Applications of Mass Spectrometry in Polymer Analysis: Use of GC-GC-High Resolution MS to Identify Photo- and Oxidative Degradation Products of BPA-Polycarbonate..... 394
limit of detection on 2,4.6-Trinitrotoluene (TNT) by Mass Spectrometry..... 428
lipid measurements..... 331
Liposome-Based Flow Injection Immunoassay System..... 663
Lipponen, Maija and Rolf Rosenberg, Quality Control in Routine Instrumental Epithermal Neutron Activation Analysis of Geological Samples..... 224
Little, James N., The Role of Robotics in the Laboratory of the 80s,..... 191
Locascio-Brown, Laurie, Anne L. Plant, and Richard A. Durst, Liposome-Based Flow Injection Immunoassay System..... 663
Lochmuller, C. H., The Role of the Robot in the Chemical Laboratory..... 267
Lorch, V, L. J. Moore, J. E. Parks, M. T. Spaar, D. W. Beekman, and E. H. Taylor, Ultra-Trace Elemental and Isotopic Quantification for Neonatal Nutrition Studies..... 328
lower oxygenated organic compounds..... 299
luminescence measurements..... 438

M

Magee, Charles, W., Depth Profiling of Trace Constituents Using Secondary Ion Mass Spectrometry..... 390
major, minor, and trace elemental nutrients..... 354

Malinowski, E. R., K. Schostack, P. Parekh, and S. Patel, Evolutionary Factor Analysis 256
manganese in serum 323
Markides, Karin E., Milton L. Lee, and Nebojsa Djordjevic, Supercritical Fluid Chromatography: Application to Trace Analysis 409
Marković, Milenko, Nevenka Pavković, and Neven D. Pavković, Precipitation of $NH_4UO_2PO_4 \cdot 3H_2O$—Solubility and Structural Comparison with Alkali Uranyl(2+) Phosphates... 557
Marshall, J. C., and T. L. Isenhour, Expert Systems and Robotics 209
Martinez, Richard I., Absolute Cross-Section Measurements in XQQ Instruments: The NBS Round Robin 431
Martire, Daniel E., Michele (Miller) Schantz, and B. N. Barman, Partitioning of Alkylbenzenes and Aliphatic Alcohols between Hexadecane and Methanol-Water Mixtures 161
mass 565
mass spectrometer technique 419
mass spectrometry 249, 428
mass spectrometry, glow discharge 392
mass spectrometry in polymer analysis 394
Massey, R., D. J. McWeeny, J. R. Dean, and H. M. Crews, Trace Element Speciation in Food: A Combined Enzymolysis—SEC-ICP-MS Approach 349
Massey, R. C., D. J. McWeeny, J. R. Dean, L. Ebdon, and H. M. Crews, Some Applications of Isotope Analysis of Lead in Food by ICP-MS 464
Massey, R. C., D. J. McWeeny, I. Parker, M. Scotter, J. R. Startin, M. J. Dennis, and N. Howarth, Ethyl Carbamate Analysis in Fermented Products: A Comparsion of Measurements of Mass Spectrometry, Thermal Energy Analyser, and Hall Electrolytic Conductivity Detector 249
Material Handling Workstation 539
material properties 61
material purity 396
May, Ralph J., Woodfin V. Ligon, Jr., and Arnold Factor, Applications of Mass Spectrometry in Polymer Analysis: Use of GC-GC-High Resolution MS to Identify Photo- and Oxidative Degradation Products of BPA-Polycarbonate 394
McGown, Linda B., and Kasem Nithipatikom, Sodium Taurocholate Micelles in Fluorometrix Analysis 443
McKinney, Gerald L., Precision and Bias of Graphite Furnace Analysis of Environmental Samples 307
McLeod, C. W., Y. Zhang, I. Cook, A. Cox, A. R. Date, and Y. Y. Cheung, Flow Injection-Inductively Coupled Plasma Spectrometry: A New Strategy for Ultratrace Analysis 462
McSparron, Donald A., James H. Walker, Robert D. Saunders, and John K. Jackson, The NBS Scale of Spectral Irradiance 7
McWeeny, D. J., J. R. Dean, L. Ebdon, H. M. Crews, and R. C. Massey, Some Applications of Isotope Analysis of Lead in Food by ICP-MS 464
McWeeny, D. J., I. Parker, M. Scotter, J. R. Startin, M. J. Dennis, N. Howarth, and R. C. Massey, Ethyl Carbamate Analysis in Fermented Products: A Comparsion of Measurements of Mass Spectrometry, Thermal Energy Analyser, and Hall Electrolytic Conductivity Detector 249
McWeeny, D. J., J. R. Dean, H. M. Crews, and R. Massey, Trace Element Speciation in Food: A Combined Enzymolysis—SEC-ICP-MS Approach 349
measurement 643
Measurement of Sunlight-Induced Transient Species in Surface Waters 285
Measurement of the Universal Gas Constant *R* Using a Spherical Acoustic Resonator 85
measurements in XQQ instruments 431
measuring machine 41
Mehl, J. B., R. S. Davis, M. R. Moldover, J. P. M. Trusler, and T. J. Edwards, Measurement of the Universal Gas Constant *R* Using a Spherical Acoustic Resonator 85
mercury 85
methanol-water mixtures 161
metrology 41
MeV Ion Beam Analysis 473
Michaelis, Markus, Wolfhard Wegscheider, and Hugo M. Ortner, Improving Accuracy in Graphite Furnace Atomic Absorption Spectrometry Through Peak Shape Monitoring 467
Michalko, P. M., J. H. Frost, J. H. Phillips, and C. A. Potera, The Use of Cryogenic Size Reduction to Improve Purgeable Priority Pollutant Analyses in Soil Samples 292
microanalysis 372, 377
microelectronics constituent materials 398
micrometer scale 518
microscope 374
Microwave Acid Sample Decomposition for Elemental Analysis 269
Microwave Induced Plasmas as Sources for Atomic Spectroscopy 447
Miller, J. M., E. White V, P. Ellerbe, and L. T. Sniegoski, An Isotope Dilution Mass Spectrometric (IDMS) Method for the Determination of Vitamin C in Milk 367
Miller, M. K., Analysis at the Atomic Level: The Atom Probe Field-Ion Microscope 374
Miller-Ihli, Nancy J., Trace Element Determinations in Biologicals Using Atomic Absorption Spectrometry 350
mixing ratio 551
modular programming 145
molar gas constant 85
Moldover, M. R., J. P. M. Trusler, T. J. Edwards, J. B. Mehl, and R. S. Davis, Measurement of the Universal Gas Constant *R* Using a Spherical Acoustic Resonator 85
molecular fragmentation 437
Monfre, Steven L., Steven D. Brown, Todd Q. Barker, and Harlan R. Wilk, Multicomponent Analysis in Static and Flow Systems Using Digital Filters 253

monochromatic diffraction imaging 577
Moore, L. J., J. E. Parks, M. T. Spaar, D. W. Beekman, E. H. Taylor, and V. Lorch, Ultra-Trace Elemental and Isotopic Quantification for Neonatal Nutrition Studies 328
Moore, L. J., W. M. Fairbank, Jr., J. M. R. Hutchinson, J. E. Parks, and M. T. Spaar, Direct Solids Analysis Using Sputter Initiated Resonance Ionization Spectroscopy (SIRIS)..... 383
Mori, Eiji, Hideo Saisho, Masataka Tanaka, and Koichi Nakamura, Determination of Traces of Uranium and Thorium in Microelectronics Constituent Materials..... 398
Morrison, George H., Trace Analysis by Degrees: An Academic Perspective..... 187
multi-processor..... 539
multi-programming..... 145
multi-purpose biological reference materials..... 360
Multicomponent Analysis in Static and Flow Systems Using Digital Filters 253
multidimensional luminescence measurements through Cyclodextrin Complexation..... 438
Multitechnique Approach to Trace Characterization of High Purity Materials: Gallium..... 400

N

Nagy, Lajos György, Péter Zagyvai, and József Solymosi, A Uniform Concept for Error Estimation in Gamma-Ray Spectrometry.... 481
Nakamura, Koichi, Eiji Mori, Hideo Saisho, and Masataka Tanaka, Determination of Traces of Uranium and Thorium in Microelectronics Constituent Materials..... 398
Nashman, Marilyn, and Karen J. Chaconas, The NBS Vision System in the AMRF 539
Natarajan, S., J. Arunachalam, S. Jaikumar, S. V. Burangey, and S. Gangadharan, Multitechnique Approach to Trace Characterization of High Purity Materials: Gallium..... 400
NBS Round Robin..... 431
NBS Scale of Spectral Irradiance, The 7
NBS Vision System in the AMRF, The..... 539
Neal, S. L., I. M. Warner, G. Nelson. G. Patonay, and L. Blyshak, Enhanced Multidimensional Luminescence Measurements Through Cyclodextrin Complexation 438
Nelson, G., G. Patonay, L. Blyshak, S. L. Neal, and I. M. Warner, Enhanced Multidimensional Luminescence Measurements Through Cyclodextrin Complexation 438
neonatal nutrition studies 328
Nestrick, T. J., and L. L. Lamparski, Accuracy in the Determination of Chlorinated Dibenzo-p-Dioxins and Dibenzofurans in Environmental Samples..... 241
New River Sediment Standard Reference Material, A 234
Newbury, Dale E., Quantitative Compositional Mapping on a Micrometer Scale..... 518
Nieman, Timothy A., Chemiluminescence Detection in Flowing Streams—Immobilized and Solid-State Reagents..... 501
Nithipatikom, Kasem, and Linda B. McGown, Sodium Taurocholate Micelles in Fluorometrix Analysis..... 443
nitroarenes..... 279
nonfluorescent compounds via molecular fragmentation..... 437
nonlinear laser spectroscopy..... 440
Nozaki, T., Accuracy in CPAA for C, N and O and in ERDA and NRA for H 482
nuclear data analysis 479
nuclides from submicrogram quantities of biological macromolecules and xenobiotics..... 419

O

octacalcium phosphate 613
Octacalcium Phosphate Solubility Product from 4 to 37 °C..... 613
O'Haver, T. C., M. S. Epstein, R. E. Jenkins, and K. S. Epler, Automation and Application of a Direct-Current Plasma Emission Spectrometer..... 458
O'Lear, J. R., C.-j. Chang, and R. G. Cooks, Alkylation of DNA In Vivo: Development of Analytical Methodology for Trace Quantitative Analysis..... 419
Olson, T. K., C. M. Gordon, and C. W. Peters, A Fast-Neutron Diagnostic Probe 484
Open Tubular Liquid Chromatography and the Analysis of Single Neurons 403
opto-acoustic..... 643
Organic Microanalysis of Submicrogram Samples.... 245
organic serum constituents..... 341
Ortner, Hugo M., Markus Michaelis, and Wolfhard Wegscheider, Improving Accuracy in Graphite Furnace Atomic Absorption Spectrometry Through Peak Shape Monitoring..... 467
Ott, William R., Jules Z. Klose, and J. Mervin Bridges, Radiometric Calibrations of Portable Sources in the Vacuum Ultraviolet..... 21

P

PAH..... 279
Parekh, P., S. Patel, E. R. Malinowski, and K. Schostack, Evolutionary Factor Analysis..... 256
Parker, I., M. Scotter, J. R. Startin, M. J. Dennis, N. Howarth, R. C. Massey, and D. J. McWenny, Ethyl Carbamate Analysis in Fermented Products: A Comparsion of Measurements of Mass Spectrometry, Thermal Energy Analyser, and Hall Electrolytic Conductivity Detector 249

Parks, J. E., M. T. Spaar, D. W. Beekman, E. H. Taylor, V. Lorch, and L. J. Moore, Ultra-Trace Elemental and Isotopic Quantification for Neonatal Nutrition Studies 328
Parks, J. E., M. T. Spaar, L. J. Moore, W. M. Fairbank, Jr., and J. M. R. Hutchinson, Direct Solids Analysis Using Sputter Initiated Resonance Ionization Spectroscopy (SIRIS) 383
Parlanti, E., M. Ewald, and P. Garrigues, Trace Analysis of Aromatic Compounds in Natural Samples by Shpol'skii Spectroscopy 441
partition coefficients 161
Partitioning of Alkylbenzenes and Aliphatic Alcohols between Hexadecane and Methanol-Water Mixtures 161
Paschal, Daniel C., and George G. Bailey, Determination of Manganese in Serum with Zeeman Effect Graphite Furnace Atomic Absorption 323
Patel, S., E. R. Malinowski, K. Schostack, and P. Parekh, Evolutionary Factor Analysis 256
Patonay, G., L. Blyshak, S. L. Neal, I. M. Warner, and G. Nelson, Enhanced Multidimensional Luminescence Measurements Through Cyclodextrin Complexation 438
Pattern Recognition Classification and Identification of Trace Organic Pollutants in Ambient Air from Mass Spectra 281
Patterson, D. G., S. J. Smith, and J. S. Holler, Quantification of Toxic Chemicals in Selected Human Populations 412
Pavković, Neven D., Nevenka Pavković, and Milenko Marković, Precipitation of $NH_4UO_2PO_4.3H_2O$—Solubility and Structural Comparison with Alkali Uranyl(2+) Phosphates 557
Pavković, Nevenka, Neven D. Pavković, and Milenko Marković, Precipitation of $NH_4UO_2PO_4.3H_2O$—Solubility and Structural Comparison with Alkali Uranyl(2+) Phosphates 557
PCB 343
PCB Identification System 298
pesticide 298, 343
Peters, C. W., T. K. Olson, and C. M. Gordon, A Fast-Neutron Diagnostic Probe 484
Petersen, W., M. H. Salehi, T. Dietrich, A Knöchel, M. Bavdaz, N. Gurker, and P. Ketelsen, Synchrotron Radiation Excited Fluorescence Micro-Analysis Using a New Imaging Technique 379
Peterson, James C., and Peter Robinson, Recent Advances in the Analysis of PCBs and Pesticides in Human Adipose Tissue 343
Pharmaceutical Trace Analysis 242
phase angle 53
phase angle standard 53
phase meter 53
Phase Meter Calibration at NBS 53
phenyltin Compounds 301
Phillips, John G., Donald W. Thayer, Jay B. Fox, Jr., Ronald K. Jenkins, and Stanley A. Ackerman, Effects of Ionizing Radiation on Nutrients in Foods 364
Phillips, J. H., C. A. Potera, P. M. Michalko, and J. H. Frost, The Use of Cryogenic Size Reduction to Improve Purgeable Priority Pollutant Analyses in Soil Samples 292
piston-gage 565
Plant, Anne, L., Richard A. Durst, and Laurie Locascio-Brown, Liposome-Based Flow Injection Immunoassay System 663
plasma-mass spectrometry 433
plume 603
point source heater 603
Potera, C. A., P. M. Michalko, J. H. Frost, and J. H. Phillips, The Use of Cryogenic Size Reduction to Improve Purgeable Priority Pollutant Analyses in Soil Samples 292
Powell, C. J., The Accuracy of Surface Analyses 387
Practical Uncertainty Limits to the Mass Determination of a Piston-Gage Weight 565
pre-column derivatization 504
precipitation 557
Precipitation of $NH_4UO_2PO_4.3H_2O$—Solubility and Structural Comparison With Alkali Uranyl(2+) Phosphates 557
Precision and Bias of Graphite Furnace Analysis of Environmental Samples 307
pressure standards 545
primary standards 545
Process Analytical Chemistry 207
Prospects for Trace Analysis in the Analytical Electron Microscope 369
purgeable priority pollutant analyses 292

Q

quality assurance 232
quality assurance materials for the analysis of environmental pollutants 237
quality control for trace analysis 221
Quality Control in Routine Instrumental Epithermal Neutron Activation Analysis of Geological Samples 224
quantification of food contaminants 365
Quantification of Toxic Chemicals in Selected Human Populations 412
Quantitation of Arsenic Species in Urine for Exposure Assessment Studies 315
Quantitative Aspects of Glow Discharge Mass Spectrometry 426
Quantitative Compositional Mapping on a Micrometer Scale 518
quantitative electron probe microanalysis 509
Quantitative Secondary Ion Mass Spectrometry 510

quantitative trace analysis in industry today 189
Quintiere, J. G., The Application of Flame Spread Theory to Predict Material Performance 61

R

R 85
radiance 21
Radiometric Calibrations of Portable Sources in the Vacuum Ultraviolet 21
radiometry 7, 21
Range-Programming Stripping Voltammetry for Determination of Some Metals in Seawater 296
Rasberry, Stanley D., Accuracy in Analysis: The Role of Standard Reference Materials 213
reaction interface 419
Recent Advances in the Analysis of PCBs and Pesticides in Human Adipose Tissue 343
reduced palladium 450
reference parameters 326
real-time 539
Real-Time Control System 539
Relative Sensitivity and Quantitation in Glow Discharge Mass Spectrometry: A Progress Report 392
Reliable Measurement of Major, Minor, and Trace Elemental Nutrients 354
reliable temperature controller 533
resonator 85
response linearity 7
Rettberg, T. M., D. E. Shrader, and L. M. Beach, Graphite Furnace AAS: Application of Reduced Palladium as a Chemical Modifier 450
reversed phase liquid chromatography 161
Rice, C. D., R. G. Huggett, M. A. Unger, and F. A. Espourteille, Determination of Tributyltin in the Marine Environment 277
Richard, John J., and Gregor A. Junk, Solid Phase Extraction on a Small Scale 274
Robinson, Peter, and James C. Peterson, Recent Advances in the Analysis of PCBs and Pesticides in Human Adipose Tissue 343
robotics and expert systems 209
robotics in radiation environments 268
robotics in the laboratory 191
Role of the Robot in the Chemical Laboratory, The 267
Role of Robotics in the Laboratory of the 80s, The 191
Rosenberg, Rolf, and Maija Lipponen, Quality Control in Routine Instrumental Epithermal Neutron Activation Analysis of Geological Samples 224
round robins 545
Ruf, H., K. Schorb, H. J. Ache, and J. M. Torres Llosa, Stripping Voltammetric Assay of Trace Technetium with a TOPO Coated Glassy Carbon Electrode 493
Ruimin, Liu, and Bruce F. Field, An Improvement in the Reliability of Standard Cell Enclosures 533
Rukkers, J. M., and T. J. Buckley, A Computer Controlled Data Acquistion System for Combustion Calorimetric Experiments 145

S

Saisho, Hideo, Masataka Tanaka, Koichi Nakamura, and Eiji Mori, Determination of Traces of Uranium and Thorium in Microelectronics Constituent Materials 398
Salehi, M. H., T. Dietrich, A. Knöchel M. Bavdaz, N. Gurker, P. Ketelsen, and W. Petersen, Synchrotron Radiation Excited Fluorescence Micro-Analysis Using a New Imaging Technique 379
Sanderson, N. E., P. Charalambous, D. J. Hall, and R. Brown, Quantitative Aspects of Glow Discharge Mass Spectrometry 426
Santoliquido, Patricia, M., The Determination of Trace Elements in Uranium Oxide (U_3O_8) by Inductively Coupled Plasma Emission Spectrometry and Graphite Furnace Atomic Absorption Spectrometry 452
Saunders, Robert D., John K. Jackson, Donald A. McSparron, and James H. Walker, The NBS Scale of Spectral Irradiance 7
Savory, John, Michael Kinter, David A. Herold, Judy C. Hundley, and Michael R. Wills, Use of High Resolution GC/MS for Obtaining Accuracy in Lipid Measurements 331
Schaffer, R., L. T. Sniegoski, E. White V, M. J. Welch, A. Cohen, and P. Ellerbe, The Development of Definitive Methods for Organic Serum Constituents 341
Schantz, Michele (Miller), B. N. Barman, and Daniel E. Martire, Partitioning of Alkylbenzenes and Aliphatic Alcohols between Hexadecane and Methanol-Water Mixtures 161
Schorb, K., H. J. Ache, J. M. Torres Llosa, and H. Ruf, Stripping Voltammetric Assay of Trace Technetium with a TOPO Coated Glassy Carbon Electrode 493
Schostack, K., P. Parekh, S. Patel, and E. R. Malinowski, Evolutionary Factor Analysis 256
Scott, Donald R., William J. Dunn III, and S. L. Emery, Pattern Recognition Classification and Identification of Trace Organic Pollutants in Ambient Air from Mass Spectra 281
Scotter, M., J. R. Startin, M. J. Dennis, N. Howarth, R. C. Massey, D. J. McWenny, and I. Parker, Ethyl Carbamate Analysis in Fermented Products: A Comparsion of Measurements of Mass Spectrometry, Thermal Energy Analyser, and Hall Electrolytic Conductivity Detector 249
SEC-ICP-MS approach 349
secondary ion mass spectrometry 390, 510

Seegopaul, Purneshwar, and Maria C. L. Williams, Characterization of High Purity Silicides 239
Seegopaul, Purneshwar, Analytical Chemistry and Material Purity in the Semiconductor Industry 396
semiconductor industry 396
sensitivity and quantitation 392
Sequential Automated Analysis System for Lower Oxygenated Organic Compounds in Ambient Air 299
Sheffield, Ann E., Lloyd A. Currie, and George A. Klouda, Trace Radiocarbon Analysis of Environmental Samples 289
Shpol'skii Spectroscopy 441
Shrader, D. E., L. M. Beach, and T. M. Rettberg, Graphite Furnace AAS: Application of Reduced Palladium as a Chemical Modifier 450
Sieck, B., W. E. Brown, M. S. Tung, and N. Eidelman, Octacalcium Phosphate Solubility Product from 4 to 37 °C 613
SIMS 499
single neurons 403
SIRIS 383
Slavin, W., Accuracy in Furnace Atomic Absorption Spectroscopy 445
slit-scattering function 7
small scale fire tests 61
Smith, J., S. Ahuja, and G. Thompson, Trace/Ultratrace Analyses of Unstable Compounds: Investigations on Hydrazobenzene and Azobenzene 344
Smith, S. J., J. S. Holler, and D. G. Patterson, Quantification of Toxic Chemicals in Selected Human Populations 412
Sniegoski, L. T., E. White V, and G. D. Byrd, Determination of 3-Quinuclidinyl Benzilate in Urine 293
Sniegoski, L. T., E. White V, M. J. Welch, A. Cohen, P. Ellerbe, and R. Schaffer, The Development of Definitive Methods for Organic Serum Constituents 341
Sniegoski, L. T., J. M. Miller, E. White V, and P. Ellerbe, An Isotope Dilution Mass Spectrometric (IDMS) Method for the Determination of Vitamin C in Milk 367
Sodium Taurocholate Micelles in Fluorometrix Analysis 443
Solid Phase Extraction on a Small Scale 274
solid-state reagents 501
solubility 613
solubility product 557, 613
Solvent-Free Injection in Supercritical Fluid Chromatography Using Sintered Glass Deposition 655
Solymosi, József, Péter Zagyvai, and Lajos György Nagy, A Uniform Concept for Error Estimation in Gamma-Ray Spectrometry 481
Some Applications of Isotope Analysis of Lead in Food by ICP-MS 464
Some Atomic Asborption Spectrometric Applications to Clinical-Biomedical Trace Metal Analyses 334
Spaar, M. T., D. W. Beekman, E. H. Taylor, V. Lorch, L. J. Moore and J.E. Parks, Ultra-Trace Elemental and Isotopic Quantification for Neonatal Nutrition Studies 328
Spaar, M. T., L. J. Moore, W. M. Fairbank, Jr., J. M. R. Hutchinson, and J. E. Parks, Direct Solids Analysis Using Sputter Initiated Resonance Ionization Spectroscopy (SIRIS) 383
spectral irradiance 7
speed of sound 85
spherical resonator 85
Spiegelman, Clifford H., Robert L. Watters, Jr., and Raymond J. Carroll, Heteroscedastic Calibration Using Analyzed Reference Materials as Calibration Standards 264
sputter initiated resonance ionization spectroscopy 383
square wave voltammetry 487
St. Claire, R. L., III, J. G. White, P. R. Dluzneski, J. S. M. de Wit, J. W. Jorgenson, and R. T. Kennedy, Open Tubular Liquid Chromatography and the Analysis of Single Neurons 403
Stable Isotope Dilution GC/MS for the Quantification of Food Contaminants 365
standard cell enclosure 533
standards 7
standards and chemometrics 193
standards (radiometric) 21
standard reference materials 213
Stanley, M. S., K. L. Duffin, J. C. Dunphy, and K. L. Busch, Biochemical Applications of Chromatography/SIMS 499
Startin, J. R., M. J. Dennis, N. Howarth, R. C. Massey, D. J. McWeeny, I. Parker, and M. Scotter, Ethyl Carbamate Analysis in Fermented Products: A Comparison of Measurements of Mass Spectrometry, Thermal Energy Analyser, and Hall Electrolytic Conductivity Detector 249
Startin, James R., and John Gilbert, Stable Isotope Dilution GC/MS for the Quantification of Food Contaminants 365
static and flow systems 253
Statistical Models in Quality Control for Trace Analysis 221
Steiner, Bruce, Masao Kuriyama, Ronald C. Dobbyn, and Uri Laor, Diffraction Imaging (Topography) with Monochromatic Synchrotron Radiation 577
Stevens, Robert K., Annular Denuders and Filter Packs Designed to Measure Ambient Levels of Acidic and Basic Air Pollutants 283
Stripping Voltammetric Assay of Trace Technetium with a TOPO Coated Glassy Carbon Electrode 493
Studies of Limit of Detection on 2,4,6-Trinitrotoluene (TNT) by Mass Spectrometry 428
submicrogram samples 245
Subramanian, K. S., Determination of Chromium (III) and Chromium (VI) by Ammonium Pyrrolidine Dithiocarbamate-Methyl Isobutyl Ketone-Furnace Atomic Absorption Spectrometry 305

sunlight-induced transient species 285
Supercritical fluid chromatography 655
Supercritical Fluid Chromatography:
Application to Trace Analysis 409
supercritical fluids 655
surface analyses 387
surface effects 565
surface waters 285
Synchrotron Radiation Excited Fluorescence
Micro-Analysis Using a New Imaging
Technique 379
synchrotron topography 577

T

Tanaka, Masataka, Koichi Nakamura, Eiji Mori, and Hideo Saisho, Determination of Traces of Uranium and Thorium in Microelectronics Constituent Materials 398
Tang, C. P., M. R. Lee, S. C. Chang, and T. S. Kao, Studies of Limit of Detection on 2,4,6-Trinitrotoluene (TNT) by Mass Spectrometry 428
Tanner, James, Wayne Wolf, Rolf Zeisler, and Iyengar Venkatesh, Development of Multi-Purpose Biological Reference Materials 360
Taylor, John K., The Importance of Quality Assurance in Trace Analysis 232
Taylor, H. E., and J. R. Garbarino, Assessment of the Analytical Capabilities of Inductively Coupled Plasma-Mass Spectrometry 433
Taylor, E. H., V. Lorch, L. J. Moore, J. E. Parks, M. T. Spaar, and D. W. Beekman, Ultra-Trace Elemental and Isotopic Quantification for Neonatal Nutrition Studies 328
Technical Difficulties Associated with the Formation of Carbon-11 Labelled Carboxylic Acids 338
temperature 85
temperature protection circuit 533
temperature-regulated oven 533
Thayer, Donald W., Jay B. Fox, Jr., Ronald K. Jenkins, Stanley A. Ackerman, and John G. Phillips, Effects of Ionizing Radiation on Nutrients in Foods 364
thermal energy analyser 249
thermal radiation 61
thermistor 603
thermometry 85
Thompson, R. E., J. R. Tuschall, and T. M. Anderson, U.S. EPA Reference Standards and Quality Assurance Materials for the Analysis of Environmental Pollutants 237
Thompson, J. N., Accurate Measurement of Vitamins in Foods and Tissues 362
Thompson, G., J. Smith, and S. Ahuja, Trace/Ultratrace Analyses of Unstable Compounds: Investigations on Hydrazobenzene and Azobenzene 344
thorium and uranium in microelectronics constituent materials 398
Tilford, Charles R., International Comparisons of Pressure Standards: A Status Report 545
TNT 428
Tomboulian, P., S. M. Walters, and K. K. Brown, Trace Level Quantitation of Phenyltin Compounds Using HPTLC 301
TOPO coated glassy carbon electrode 493
Torres Llosa, J. M., H. Ruf, K. Schorb, and H. J. Ache, Stripping Voltammetric Assay of Trace Technetium with a TOPO Coated Glassy Carbon Electrode 493
toxic chemicals 412
Trace Analyses of Impurities in Povidone by Square Wave Voltammetry 487
trace analysis 175, 409
trace analysis, accuracy 217
Trace Analysis by Degrees: An Academic Perspective 187
trace analysis, inorganic 419
Trace Analysis of Aromatic Compounds in Natural Samples by Shpol'skii Spectroscopy 441
trace analysis, pharmaceutical 242
trace analysis, quality assurance 232
Trace Biogenic Amine Analysis with Pre-Column Derivatization and with Fluorescent and Chemiluminescent Detection in HPLC 504
trace characterization of high purity materials 400
trace constituents 390
trace element analysis 318
Trace Element Determinations in Biologicals Using Atomic Absorption Spectrometry 350
Trace Element Speciation in Food: A Combined Enzymolysis–SEC-ICP-MS Approach 349
trace elements in Methamphetamine Hydrochloride 469
trace elements in Uranium Oxide (U_3O_8) 452
trace level, accuracy 520
Trace Level Quantitation of Phenyltin Compounds Using HPTLC 301
trace metal analyses, clinical-biomedical 334
trace metals in marine environments 321
trace metals in precipitation 312
trace organic pollutants 281
trace quantitative analysis 419
Trace Radiocarbon Analysis of Environmental Samples 289
trace technetium 493
Trace/Ultratrace Analyses of Unstable Compounds: Investigations on Hydrazobenzene and Azobenzene 344
Transferring Accuracy to the Trace Level and Then to the Field 520
trends 321
tributyltin 277
Trusler, J. P. M., T. J. Edwards, J.B. Mehl, R. S. Davis, and M. R. Moldover, Measurement of the Universal Gas Constant *R* Using a Spherical Acoustic Resonator 85
Tung, M. S., N. Eidelman, B. Sieck, and W. E. Brown, Octacalcium Phosphate Solubility Product from 4 to 37 °C 613

Turgel, Raymond S., Phase Meter Calibration at NBS 53
Tuschall, J. R., T. M. Anderson, and R. E. Thompson, U.S. EPA Reference Standards and Quality Assurance Materials for the Analysis of Environmental Pollutants 237
two dimensional metrology 41

U

ultratrace analysis 462
Ultra-Trace Elemental and Isotopic Quantification for Neonatal Nutrition Studies 328
ultraviolet 21
Umăna, Mirtha, Jess Waller, Mansukh Wani, Carol Whisnant, and Edgar Cook, Enzyme-Enhanced Electrochemical Immunoassay for Phenytoin 659
Unger, M. A., F. A. Espourteille, C. D. Rice, and R. G. Huggett, Determination of Tributyltin in the Marine Environment 277
Uniform Concept for Error Estimation in Gamma-Ray Spectrometry, A 481
unit-cell dimensions 557
Universal Gas Constant 85
unstable compounds 344
uranium oxide (U_3O_8) 452
uranium and thorium in microelectronics constituent materials 398
U.S. EPA Reference Standards and Quality Assurance Materials for the Analysis of Environmental Pollutants 237
Use of Cryogenic Size Reduction to Improve Purgeable Priority Pollutant Analyses in Soil Samples, The 292
use of GC-GC-high relolution MS to identify photo- and oxidative degradation products of BPA-Polycarbonate 394
Uses of High Resolution GC/MS for Obtaining Accuracy in Lipid Measurements 331
Polycarbonate 394

V

vacuum standards 545
vacuum ultraviolet 21
Van Borm, W., P. Van Espen, and K. Janssens, Increased Accuracy in the Automated Interpretation of Large EPMA Data Sets by the Use of an Expert System 260
Van Espen, K. Janssens, and W. Van Borm, Increased Accuracy in the Automated Interpretation of Large EPMA Data Sets by the Use of an Expert System 260
Vanballenberghe, L., A. De Kesel, J. Hoste, B. Wallaeys, J. Vandenhaute, and J. Versieck, Biological Reference Materials for Trace Element Analysis: What is New? 318
Vandenhaute, J., J. Versieck, L. Vanballenberghe, A. De Kesel, J. Hoste, and B. Wallaeys, Biological Reference Materials for Trace Element Analysis: What is New? 318
Veber, M., V. Francetic, R. Durst, and S. Gomiscek, Electrochemical Studies of Dithiocarbamates and Related Compounds 496
Versieck, J., L. Vanballenberghe, A. De Kesel, J. Hoste, B. Wallaeys, and J. Vandenhaute, Biological Reference Materials for Trace Element Analysis: What is New? 318
vitamins in foods and tissues 362
voltammetric assay of trace technetium 493
Voltammetric Sensors Using Chemically Active Electrode Materials 488
voltammetry 296, 489

W

Walker, James H., Robert D. Saunders, John K. Jackson, and Donald A. McSparron, The NBS Scale of Spectral Irradiance 7
Wallaeys, B., J. Vandenhaute, J. Versieck, L. Vanballenberghe, A. De Kesel, and J. Hoste, Biological Reference Materials for Trace Element Analysis: What is New? 318
Waller, Jess, Mansukh Wani, Carol Whisnant, Edgar Cook, and Mirtha Umăna, Enzyme-Enhanced Electrochemical Immunoassay for Phenytoin 659
Walters, S. M., K. K. Brown, and P. Tomboulian, Trace Level Quantitation of Phenyltin Compounds Using HPTLC 301
Wang, C., T. Kuwana, T. Kawasaki, and O. Wong, Trace Biogenic Amine Analysis with Pre-Column Derivatization and with Fluorescent and Chemiluminescent Detection in HPLC 504
Wang, Joseph, Adsorptive Stripping Voltammetry—A New Electroanalytical Avenue for Trace Analysis 489
Wang, Y. L., R. Levi-Setti, and J. Chabala, Imaging Microanalysis of Materials With a Finely Focused Heavy Ion Probe 377
Wani, Mansukh, Carol Whisnant, Edgar Cook, Mirtha Umăna, and Jess Waller, Enzyme-Enhanced Electrochemical Immunoassay for Phenytoin 659
Warner, I. M., G. Nelson, G. Patonay, L. Blyshak, and S. L. Neal, Enhanced Multidimensional Luminescence Measurements Through Cyclodextrin Complexation 438
Watanabe, Ikuo, Sequential Automated Analysis System for Lower Oxygenated Organic Compounds in Ambient Air 299
water 603
water vapor 551
Watters, Robert L., Jr., Raymond J. Carroll, and Clifford H. Spiegelman, Heteroscedastic Calibration Using Analyzed Reference Materials as Calibration Standards 264
waveform analysis 643
Wegscheider, Wolfhard, Hugo M. Ortner, and Markus Michaelis, Improving Accuracy in Graphite Furnace Atomic Absorption Spectrometry Through Peak Shape Monitoring 467

Wegscheider, Wolfhard, Chemometrics in Europe: Selected Results 257
Wehmeyer, Kenneth R., Matthew J. Doyle, D. Scott Wright, H. Brian Halsall, William R. Heineman, and Sarah H. Jenkins, Electrochemical Enzyme Immunoassay 491
Wehry, E. L., Fluorescence Spectrometric Determination of Nonfluorescent Compounds via Molecular Fragmentation 437
weighing 565
weighing errors 565
Welch, B. E., and R. S. Davis, Practical Uncertainty Limits to the Mass Determination of a Piston-Gage Weight 565
Welch, M. J., A. Cohen, P. Ellerbe, R. Schaffer, L. T. Sniegoski, and E. White V, The Development of Definitive Methods for Organic Serum Constituents 341
Westgard, James O., Design of Cost-Effective QC Procedures for Clinical Chemistry 218
Whisnant, Carol, Edgar Cook, Mirtha Umãna, Jess Waller, and Mansukh Wani, Enzyme-Enhanced Electrochemical Immunoassay for Phenytoin 659
White, D. R., J. F. Alofs, and D. E. Hagen, Condensation Method for Humidity Measurement in the UMR Cloud Simulation Chamber 551
White, E., V, G. D. Byrd, and L. T. Sniegoski, Determination of 3-Quinuclidinyl Benzilate in Urine 293
White, E., V, M. J. Welch, A. Cohen, P. Ellerbe, R. Schaffer, and L. T. Sniegoski, The Development of Definitive Methods for Organic Serum Constituents 341
White, E., V, P. Ellerbe, L. T. Sniegoski and J. M. Miller, An Isotope Dilution Mass Spectrometric (IDMS) Method for the Determination of Vitamin C in Milk 367
White, J. G., P. R. Dluzneski, J. S. M. de Wit, J. W. Jorgenson, R. T. Kennedy, and R. L. St. Claire III, Open Tubular Liquid Chromatography and the Analysis of Single Neurons 403
Wilk, Harlan R., Steven L. Monfre, Steven D. Brown, and Todd Q. Barker, Multicomponent Analysis in Static and Flow Systems Using Digital Filters 253
Williams, D. B., Prospects for Trace Analysis in the Analytical Electron Microscope 369
Williams, Maria C. L., and Seegopaul Purneshwar, Characterization of High Purity Silicides 239
Wills, Michael R., John Savory, Michael Kinter, David A. Herold, and Judy C. Hundley, Use of High Resolution GC/MS for Obtaining Accuracy in Lipid Measurements 331
Winer, Arthur M., Janet Arey, Barbara Zielinska, and Roger Atkinson, Analysis of Gaseous and Particle-Associated PAH and Nitroarenes in Ambient Air 279
Wolf, Wayne, Rolf Zeisler, Venkatesh Iyengar, and James Tanner, Development of Multi-Purpose Biological Reference Materials 360
Wong, O., C. Wang, T. Kuwana, and T. Kawasaki, Trace Biogenic Amine Analysis with Pre-Column Derivatization and with Fluorescent and Chemiluminescent Detection in HPLC 504
Wright, D. Scott, H. Brian Halsall, William R. Heineman, Sarah H. Jenkins, Kenneth R. Wehmeyer, and Matthew J. Doyle, Electrochemical Enzyme Immunoassay 491
Wright, John C., High Resolution Nonlinear Laser Spectroscopy 440

X

xenobiotics 419
XQQ instruments 431
x-ray diffraction pattern 557

Y

Yeung, Edward S., Applications of Lasers in Bioanalytical Chemistry 502

Z

Zagyvai, Péter, Lajos György Nagy, and Jozsef Sólymosi, A Uniform Concept for Error Estimation in Gamma-Ray Spectrometry 481
Zeeman Effect 323
Zeisler, Rolf, Venkatesh Iyengar, James Tanner, and Wayne Wolf, Development of Multi-Purpose Biological Reference Materials 360
Zhang, Y., I. Cook, A. Cox, A.R. Date, Y. Y. Cheung, and C. W. McLeod, Flow Injection-Inductively Coupled Plasma Spectrometry: A New Strategy for Ultratrace Analysis 462
Zielinska, Barbara, Roger Atkinson, Arthur M. Winer, and Janet Arey, Analysis of Gaseous and Particle-Associated PAH and Nitroarenes in Ambient Air 279